Accepted Manuscript

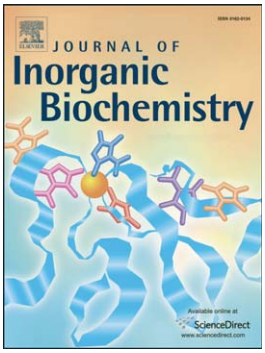

Structure-Specific Adipogenic Capacity of Novel, Well-defined Ternary Zn(II)-Schiff Base Materials. Biomolecular Correlations in Zinc-Induced Differentiation of 3 T3-L1 Pre-adipocytes to Adipocytes

O. Tsave, E. Halevas, M.P. Yavropoulou, A. Kosmidis Papadimitriou, J.G. Yovos, A. Hatzidimitriou, C. Gabriel, V. Psycharis, A. Salifoglou

PII: S0162-0134(15)30057-X
DOI: doi: 10.1016/j.jinorgbio.2015.08.014
Reference: JIB 9785

To appear in: *Journal of Inorganic Biochemistry*

Received date: 16 June 2015
Revised date: 2 August 2015
Accepted date: 5 August 2015

Please cite this article as: O. Tsave, E. Halevas, M.P. Yavropoulou, A. Kosmidis Papadimitriou, J.G. Yovos, A. Hatzidimitriou, C. Gabriel, V. Psycharis, A. Salifoglou, Structure-Specific Adipogenic Capacity of Novel, Well-defined Ternary Zn(II)-Schiff Base Materials. Biomolecular Correlations in Zinc-Induced Differentiation of 3 T3-L1 Pre-adipocytes to Adipocytes, *Journal of Inorganic Biochemistry* (2015), doi: 10.1016/j.jinorgbio.2015.08.014

This is a PDF file of an unedited manuscript that has been accepted for publication. As a service to our customers we are providing this early version of the manuscript. The manuscript will undergo copyediting, typesetting, and review of the resulting proof before it is published in its final form. Please note that during the production process errors may be discovered which could affect the content, and all legal disclaimers that apply to the journal pertain.

ACCEPTED MANUSCRIPT

Structure-Specific Adipogenic Capacity of Novel, Well-defined Ternary Zn(II)-Schiff Base Materials. Biomolecular Correlations in Zinc-Induced Differentiation of 3T3-L1 Pre-adipocytes to Adipocytes.

O. Tsave,[a] E. Halevas,[a] M. P. Yavropoulou,[d] A. Kosmidis Papadimitriou,[a] J. G. Yovos,[d] A. Hatzidimitriou,[b] C. Gabriel,[a,e] V. Psycharis,[c] A. Salifoglou[a]*

[a] Laboratory of Inorganic Chemistry, Department of Chemical Engineering, Aristotle University of Thessaloniki, Thessaloniki 54124, Greece

[b] Laboratory of Inorganic Chemistry, Department of Chemistry, Aristotle University of Thessaloniki, Thessaloniki 54124, Greece

[c] Institute of Advanced Materials, Physicochemical Processes, Nanotechnology and Microsystems, Department of Materials Science, N.C.S.R. "Demokritos", Aghia Paraskevi 15310, Attiki, Greece

[d] Laboratory of Clinical and Molecular Endocrinology, 1st Department of Internal Medicine, AHEPA, University Hospital, Aristotle University of Thessaloniki, Thessaloniki 54124, Greece

[e] Center for Research of the Structure of Matter, Magnetic Resonance Laboratory, Department of Chemical Engineering, Aristotle University of Thessaloniki, Thessaloniki 54124, Greece

* Author to whom correspondence should be addressed.

Tel: +30-2310-996-179 Fax: +30-2310-996-196 E-mail: salif@auth.gr

ACCEPTED MANUSCRIPT

Abstract

Among the various roles of zinc discovered to date, its exogenous activity as an insulin mimetic agent stands as a contemporary challenge currently under investigation and a goal to pursue in the form of a metallodrug against type 2 Diabetes mellitus. Poised to investigate the adipogenic potential of Zn(II) and appropriately configure its coordination sphere into well-defined anti-diabetic forms, a) a series of new well-defined ternary dinuclear Zn(II)-L (L = Schiff base ligands with a variable number of alcoholic moieties) compounds were synthesized and physicochemically characterized, c) their cytotoxicity and migration effect(s) in both pre- and mature adipocytes was assessed, d) their ability to effectively induce cell differentiation of 3T3-L1 pre-adipocytes into mature adipocytes was established, and d) closely linked molecular targets involving or influenced by the specific Zn(II) forms were perused through molecular biological techniques, cumulatively delineating factors involved in Zn(II)-induced adipogenesis. Collectively, the results a) reveal the significance of key structural features of Schiff ligands coordinated to Zn(II), thereby influencing its (a)toxicity behavior and insulin-like activity, b) project molecular targets influenced by the specific forms of Zn(II) formulating its adipogenic potential, and c) exemplify the interwoven relationship between Zn(II)-L structural speciation and insulin mimetic biological activity, thereby suggesting ways of fine tuning structure-specific zinc-induced adipogenicity in future efficient antidiabetic drugs.

Keywords: Schiff ligand-based zinc reactivity, zinc metallodrugs, structure-specific bioactivity selection, fine-tuning zinc insulin-like activity, zinc-induced adipogenesis, biomolecular correlations

ACCEPTED MANUSCRIPT

ACCEPTED MANUSCRIPT

1. Introduction

Diabetes Mellitus (DM) is a group of metabolic diseases characterized by hyperglycemia due to absence of insulin or impaired insulin secretion. Chronic hyperglycemia in diabetes is associated with long-term micro and macrovascular complications, significantly increasing mortality and morbidity of diabetic patients. DM is generally classified into two types: a) type 1 or insulin-dependent type, caused by autoimmune destruction of pancreatic beta cells, and b) type 2 or non-insulin dependent, caused by the dysfunction of beta cells and insulin resistance, which is due to the inability of insulin target tissues to respond properly to insulin [**1**-**5**]. Insulin action involves an intracellular signaling cascade, initiated by insulin binding to its trans-membrane receptor, resulting in receptor autophosphorylation, through activation of the receptor tyrosine kinase, and phosphorylation of insulin receptor substrates (IRSs). In turn, phosphorylated IRS activates downstream kinases, such as phosphatidylinositol 3-kinase (PI3K) and Akt kinase, both essential for insulin-induced glucose transport in the periphery. Although the underlying mechanisms of insulin resistance are not completely understood, impaired insulin-dependent PI3K activation and downstream signaling is considered the convergence point of insulin dysfunction. Insulin resistance of peripheral target tissues is caused by a reduced number of functional glucose transporters (GLUTs), mainly GLUT 4. In murine cells, the defect appears to emerge through failure of bound vesicle carriers to displace the cytoplasmic membrane in response to insulin. In adipocytes the displacement is also limited, but the main mechanism of insulin resistance in these cells is the pre-translational depletion of mRNA for GLUT 4 transporters [**6,7**].

Zinc is an important trace element critical to the function of over 300 enzymes [**8,9**] and plays an important role in processes like DNA/RNA synthesis, cell division and apoptosis, insulin synthesis, secretion and signaling [**10-14**]. In addition, zinc has been linked to DM as part of the insulin complex [**15**], and several studies have investigated the role of zinc metabolism in diabetic animals and humans. Zinc appears to play a role in modulating insulin receptor tyrosine kinase activity in the skeletal muscle of a genetic DM type 2 model mouse, similar to the action of vanadium [**16**]. Moreover, zinc was proposed to affect carbohydrate metabolism through the insulin receptor, PTP1B, and other related proteins [**17**]. In fact, zinc and DM converge at several points during metabolism in cells [**18,19**]. In 1980, zinc was found to stimulate rat adipocyte lipogenesis *in vitro*, similar to the action of insulin [**20**], and exert antidiabetic effects *in vivo* as orally given $ZnCl_2$ in rats with streptozotocin-induced diabetes and leptin-deficient mice (ob/ob mice) [**21**,**22**]. As the bioavailability of $ZnCl_2$ is relatively low, the coordination chemistry of Zn(II) ion was explored, and the first orally active insulin-

ACCEPTED MANUSCRIPT

mimetic and antidiabetic Zn(II)–picolinato complexes were proposed in 2002 [**23**]. Since then, several Zn(II) complexes with different coordination structures have been synthesized [**18**-**24**].

In an effort to identify new anti-diabetic drugs containing Zn(II) and fulfilling the basic criteria of a) atoxic behavior, and b) optimal insulin mimetic activity, due attention was paid to well-defined organic substrates, which appear to play a major role in formulating Zn(II) insulin mimetic activity. They, thus, attracted our attention as potential Zn(II) binders [**25**]. Among such organic reagents, Schiff bases a) possess structural similarities with natural biological substances, b) are synthesized through relatively simple preparation procedures, and c) present valuable structural flexibility, enabling design of suitable (bio)chemical reactivity properties [**26,27**]. They have been widely studied [**28**] because of their role as intermediates in a number of enzymatic reactions and non-enzymatic glycosylations [**29**], and their industrial, antifungal, antibacterial, anticancer, antidiabetic, antiviral and herbicidal applications [**30,31,32,33,34,35**].

Guided by the idea that properly designed Schiff bases may promote Zn(II) binding, thereby giving rise to bioactive ternary Zn(II)-L-(L') insulin mimetic compounds [**30,31,32**] capable of reducing blood glucose levels, efforts were launched to a) design and synthesize well-defined ternary Zn(II)-Schiff base compounds of specific structure (organic substrates bearing systematically varying number of alcohol moieties attached to a vanillin core) and characterize them physicochemically, b) investigate their ability to induce 3T3-L1 fibroblast to mature adipocyte differentiation, c) examine the insulin mimetic potency of such compounds and determine *in vitro* their arising biological activity profile(s), d) investigate the interactions of such molecules with specific molecular targets in the insulin-induced glucose catabolic pathways known to date, and e) correlate chemical and structural features of the ternary Zn(II) compounds with the observed activities at the cellular level, thereby formulating biological activity profile-physicochemical factor relationships that enable development of optimal Zn(II) insulin mimetic drugs. To this end, we report herein the synthesis and physicochemical characterization of a series of newly designed ternary Zn(II)-Schiff base compounds, which are systematically studied with respect to their toxicity and potential to induce cell differentiation.

2. Experimental Section

2.1. Materials and Methods. All experiments were carried out under aerobic conditions. The following starting materials were purchased from commercial sources (Sigma, Fluka) and were used without further purification: tromethamine, 2-amino-1,3-propanediol,

ACCEPTED MANUSCRIPT

ethanolamine, o-vanillin, and zinc acetate dihydrate ($Zn(CH_3COO)_2 \cdot 2H_2O$). Solvents: ultrapure water, methanol, ethanol, diethyl ether. The compounds isolated and dried under vacuum at room temperature are air-stable.

2.2. Physical measurements. FT-Infrared spectra were recorded on a Perkin Elmer 1760X FT-infrared spectrometer. A ThermoFinnigan Flash EA 1112 CHNS elemental analyser was used for the simultaneous determination of carbon, hydrogen, and nitrogen (%). The analyser operation is based on the dynamic flash combustion of the sample (at 1800°C) followed by reduction, trapping, complete GC separation and detection of the products. The instrument is a) fully automated and controlled by PC via the Eager 300 dedicated software, and b) capable of handling solid, liquid or gaseous substances.

2.2.1. Solid-State NMR spectroscopy. High resolution solid-state CP-MAS ^{13}C NMR spectra for **1-3** were obtained on a Varian 600 MHz spectrometer operating at 150.86 MHz. In each case, a sufficient sample quantity was placed in a double resonance HX probe with a 3.2 mm rotor. The spinning rate used was 15.0 kHz at 25 °C. The RAMP-CP pulse sequence of the VnmrJ library was applied, whereby the ^{13}C spin-lock amplitude is varied linearly during CP, while the ^{1}H spin-lock amplitude is kept constant. RAMP-CP eliminates the Hartmann-Hahn matching profile dependence from the MAS spinning rate and optimizes signal intensity. The solid-state spectra were a result of the accumulation of 512 scans. The recycle delay used was 2s, the 90° pulse was 2.0 μs, and the contact time was 3.0 ms. The CH signal of adamantane was used as an external reference (37.78 ppm with respect to TMS).

2.2.2. Solution NMR Spectroscopy. Solution ^{1}H- and ^{13}C-NMR experiments for **1** and **3**, were carried out on Varian 600 MHz spectrometer. The sample concentration was ~5 mM. Freshly prepared compounds were dissolved in D_2O. Due to solubility problems for **2** at concentrations up to ~5 mM, well-resolved ^{1}H- and ^{13}C-NMR spectra could not be obtained. Carbon spectra were acquired with 5000 transients, a spectral width of 37000 Hz and a relaxation delay of 2s. Proton spectra were acquired with 128 transients and a spectral width of 9000 Hz. Experimental data were processed using VNMR routines. Spectra were zero-filled and subjected to exponential apodization prior to FT. Chemical shifts (δ) are reported in ppm, while spectra were referenced by the standard experimental setup.

2.2.3. Thermal Studies. A TA Instruments, model Q 600, system was used to run the simultaneous TGA experiments. The instrument mass precision is 0.1 μg. About 10 mg of each sample was placed in an open alumina sample pan for each experiment. A mixture of helium and high purity air (80/20 in N_2/O_2) was used at a constant flow rate of 100 mL/min, depending on the conditions required for running the experiments. During the experiments,

ACCEPTED MANUSCRIPT

the sample weight loss and rate of weight loss were recorded continuously under dynamic conditions, as a function of time or temperature, in the range 45–550 ^{o}C. Prior to activating the heating routine program, the entire system was purged with the appropriate gas for 10 min, at a rate of 400 mL/min, to ensure that the desired environment was established.

2.3. Preparation of compounds

2.3.1. Preparation of ligands L_iH (i=1-3). Ligands **L_1H, L_2H** and **L_3H** were prepared according to the literature [**36,37,38**].

2.3.2. Preparation of complex $Zn_2(L_1)(CH_3COO)_3$ (1). To a solution of o-vanillin (0.15 g, 1.0 mmol) in EtOH (10 mL) tromethamine (0.12 g, 1.0 mmol) was added under stirring. The resulting yellow solution was refluxed for two hours under continuous stirring and then cooled to room temperature. Subsequently, a solution of $Zn(CH_3COO)_2{\cdot}2H_2O$ (0.44 g, 2.0 mmol) in EtOH (10 mL) was added under continuous stirring. The resulting clear, yellowish reaction mixture was refluxed for an additional 2 h and then cooled to room temperature. Subsequently, the reaction flask was placed at 4 ^{o}C and diethyl ether was added. Two weeks later, yellow crystalline material precipitated at the bottom of the flask. The product was isolated by filtration and dried in vacuo. Yield: 0.34 g (61%). Anal. Calcd for **1**, $Zn_2(L_1)(CH_3COO)_3$ **(1)**. ($C_{18}H_{25}NO_{11}Zn_2$ M_r 562.13): C, 38.46; H, 4.48; N 2.49. Found: C, 38.38; H, 4.33; N 2.44.

2.3.3. Preparation of complex $[Zn_2(L_2)(CH_3COO)_3]{\cdot}H_2O$ (2). To a solution of o-vanillin (0.15 g, 1.0 mmol) in EtOH (10 mL) 2-amino-1,3-propanediol (0.091 g, 1.0 mmol) was added and the resulting yellow solution was refluxed for 2 h under continuous stirring. Then, it was cooled down to room temperature. Subsequently, a solution of $Zn(CH_3COO)_2{\cdot}2H_2O$ (0.22 g, 1.0 mmol) in EtOH (10 mL) was added under continuous stirring and the resulting clear, yellowish solution was refluxed for an additional 2 h. Then, it was cooled down to room temperature. Yellow crystals of the complex were grown by slow evaporation at 4 ^{o}C. The product was isolated by filtration and dried in vacuo. Yield: 0.32 g (58%). Anal. Calcd for **2**, $[Zn_2(L_2)(CH_3COO)_3]{\cdot}H_2O$ **(2)**. ($C_{17}H_{25}NO_{11}Zn_2$, M_r 550.12): C, 37.12; H, 4.58; N 2.55. Found: C, 36.98; H, 4.43; N 2.24.

2.3.4. Preparation of complex $Zn_2(L_3)_2(CH_3COO)_2$ (3). To a solution of o-vanillin (0.15 g, 1.0 mmol) in EtOH (10 mL) ethanolamine (0.060 mL, 1.0 mmol) was added and the resulting yellow solution was refluxed for 2 h. Then, it was cooled down to room temperature. Subsequently, a solution of $Zn(CH_3COO)_2 \cdot 2H_2O$ (0.22 g, 1.0 mmol) in EtOH (10 mL) was added under continuous stirring and the resulting clear, yellowish solution was refluxed for an additional 2 h. Then, it was cooled down to room temperature. Subsequently, the reaction

ACCEPTED MANUSCRIPT

flask was placed at 4 ^{o}C and diethyl ether was added. Two weeks later, yellow crystalline material precipitated at the bottom of the flask. The product was isolated by filtration and dried in vacuo. Yield: 0.22 g (35%). Anal. Calcd for **3**, $Zn_2(L_3)_2(CH_3COO)_2$ **(3)**. ($C_{24}H_{30}N_2O_{10}Zn_2$, M_r 637.27): C, 45.23; H, 4.75; N 4.40. Found: C, 45.03; H, 4.64; N 4.34.

2.4. X-ray crystal structure determination. X-ray quality crystals of compounds **1** and **3** were grown from a mixture of ethanol-diethyl ether, whereas crystals of compound **2** were grown from ethanol solutions. A crystal of **1** (0.15 × 0.30 × 0.46 mm) and **2** (0.07 × 0.09 × 0.15 mm) were taken from the mother liquor and immediately cooled to -113 ^{o}C. Diffraction measurements were made on a Rigaku R-AXIS SPIDER Image Plate diffractometer using graphite monochromated Cu Kα radiation. Data collection (ω-scans) and processing (cell refinement, data reduction and empirical absorption correction) were performed using the CrystalClear program package [**39**]. The structures were solved by direct methods using SHELXS-97 and refined by full-matrix least-squares methods on F^2 with SHELXL-97 [**40**]. In **1**, one of the terminal alcoholic oxygen atoms was found disordered and was refined anisotropically over two positions, O(5) and O(5a), with occupancy factors summing one. In both **1** and **2**, hydrogen atoms were either located by difference maps and refined isotropically or introduced at calculated positions as riding on bonded atoms.

A crystal of **3** (0.06 × 0.31 × 0.33 mm) was taken from the mother liquor and mounted at room temperature on a Bruker Kappa 2 APEX diffractometer equipped with a triumph monochromator using Mo Kα radiation. Unit cell dimensions were determined and refined by using the angular settings of at least 100 high intensity reflections (>10 σ(I)) in the range 19<2θ<40 ^{o}. Intensity data were recorded using ϕ and ω scans. All crystals presented no decay during data collection. The collected frames were integrated with the Bruker SAINT software package [**41**] using a narrow-frame algorithm. Data were corrected for absorption using the numerical method (SADABS) based on crystal dimensions [**42**]. Data refinement (full-matrix least-squares methods on F^2) and all subsequent calculations were performed using the Crystals version 14.40b program package [**43**]. The structure was solved by SUPERFLIP method [**44**]. Molecular illustrations with 50% ellipsoids probability were drawn by the Diamond 3.1 crystallographic package [**45**]. In all three structures (**1**-**3**), all non-hydrogen atoms were refined anisotropically. Crystallographic details for **1**, **2** and **3** are summarized in Table 1. Further experimental crystallographic details for **1**: $2\theta_{max}$=133^{o}; number of reflections collected/unique/used, 23907/3653 [R(int) = 0.0372]/3653; 387 parameters refined; Δ/σ = 0.000; $(\Delta\rho)_{max}/(\Delta\rho)_{min}$ = 0.448/-0.615 e/Å^3; R/R_w (for all data),

ACCEPTED MANUSCRIPT

0.0327/0.0784. Further experimental crystallographic details for **2**: $2\theta_{max}$=130°; number of reflections collected/unique/used, 23117/3577[R(int) = 0.0420]/3577; 341 parameters refined; Δ/σ = 0.002; $(\Delta\rho)_{max}/(\Delta\rho)_{min}$ = 0.580/-0.419 e/Å^3; R/R_w (for all data), 0.0297/0.0746. Further experimental crystallographic details for **3**: $2\theta_{max}$=56.2°; number of reflections collected/unique/used, 50189/6807/3666 [R(int) = 0.0438]/3666; $(\Delta\rho)_{max}/(\Delta\rho)_{min}$ = 0.88/-0.63 e/Å^3; R/R_w (for all data), 0.0547/0.0764.

2.5. Cell cultures and biological tests

2.5.1. Cell culture

Both pre- and mature adipocytes (3T3-L1) were cultured in 75 cm^2 cell culture flasks under appropriate conditions (5% CO_2 at 37 °C and standard humidity) in Dulbecco's modified Eagle's medium DMEM (Gibco), supplemented with 10% Fetal Bovine Serum (FBS) and 1% penicillin-streptomycin.

2.5.2. Induction of adipogenesis

3T3-L1 fibroblasts were differentiated into mature adipocytes according to a standard differentiation protocol [**46**]. Two days (day 0) post 70% confluency, cells were treated with 0.5 mM 3-isobutyl-1-methylxanthine (Sigma), 1.0 μM dexamethazone (Sigma) and 10 ng/mL of insulin as final concentrations in DMEM. Two days later (day 2), the cells were treated only with insulin and the medium was changed every two days. All experiments were performed on the 8th day of the differentiation process.

2.5.3. Cell viability assay

In an effort to assess cell survival rates post-stimulation with the newly synthesized zinc compounds, both 3T3-L1 pre-adipocytes and mature adipocytes differentiated with insulin as mentioned above, were seeded in 96-multi-well plates (2500 cells/well), and incubated with the title zinc compounds for 24 and 48 h in DMEM. The assay relies on the quantitation of ATP present, thereby attesting to the presence of metabolically active cells. The reagent is added to the cell culture (ratio 1:1) without removing the supernatant. The luciferase-produced luminescence signal intensity is determined with a Glomax 96 microplate luminometer (Promega Corporation, WI, USA).

2.5.4. Induction of adipogenesis with Zn(II)-compounds

3T3-L1 pre-adipocytes were differentiated into mature adipocytes with respect to a standard differentiation protocol (vide supra). Pre-adipocytes were treated with either 10 ng/mL of insulin and\or selected well-defined zinc compounds (1-25 μM). The tested compounds were dissolved in DMEM (10% FBS, 1% penicillin/streptomycin), followed by sterile filtration. In all experiments run, insulin-treated cells were used as positive control. A control group with

ACCEPTED MANUSCRIPT

no treated cells (without insulin or zinc compounds) was also included. On the 8th day of the differentiation process, cell differentiation was assessed with oil red O staining and Real-Time PCR for relative expression of PPAR-γ, GLUT 1, GLUT 3 and GLUT 4. All tests were carried out in triplicate.

2.5.5. RT-PCR assay

Total RNA was extracted from cells on the 8th day of the differentiation protocol, using Trizol reagent (LifeScience, Chemilab). Synthesis of cDNA was performed with the iScript cDNA synthesis kit (BioRad), according to manufacturer instructions. RT-PCR was run on Rotor Gene Q (Qiagen) using the QuantiTect SYBR Green PCR kit and appropriate reagents (Qiagen).

2.5.6. Cell migration assay

The inhibition of the endogenous migrating capacity of 3T3-L1 pre-adipocytes was assessed through an *in vitro* scratch assay. To this end, cells were seeded in 35 mm cell culture dishes in DMEM. When cells reached 70-80% confluency, a) a scratch in the monolayer traversing the entire diameter of each culture dish was engraved using a sterile pipette tip, and b) cells were allowed to grow in the culture medium in the presence of a final concentration of 25 μM of the title Zn(II) compounds. Cells were visualized using an Axio Observer Z1 microscope, with a 10x phase contrast water immersion objective (Carl Zeiss, GmbH Lena, Germany). Images were captured, using an AxioCam Hc camera, at two distinct time points 24 and 48 h after the scratch had been made.

2.5.7. Statistical analysis

The data were presented as average and standard error mean (SEM) values of triplicate sets of independent measurements. Mean survival rates and SEMs were calculated for each group. Absolute survival rates were calculated for each control group and one way analysis of variance (ANOVA) was performed for all pair comparisons, followed by post hoc analyses (Tukey) and Dunnet in the case of RT-PCR experiments. Degrees of significance were assessed by three different rating values: *$p<0.05$ (significant), **$p<0.01$ (highly significant) and ***$p<0.001$ (extremely significant) or non-significant ($p>0.05$).

3. Results

3.1. Synthesis. The synthetic exploration of the binary Zn(II)-Schiff base systems was based on the following Schiff base ligands **L_1H-L_3H,** synthesized from o-vanillin and tromethamine (**L_1H**), 2-amino-1,3-propanediol (**L_2H**), and ethanolamine (**L_3H**) [**36-38**], respectively. Subsequently, the $Zn_2(\mathbf{L_1})(CH_3COO)_3$ **(1)** complex was synthesized in a facile fashion from simple reagents in alcoholic solutions. In a typical reaction, $Zn(CH_3COO)_2{\cdot}2H_2O$ reacted

ACCEPTED MANUSCRIPT

with Schiff base **L_1H** using ethanol as a solvent. The overall stoichiometric reaction leading to **1** is shown schematically below:

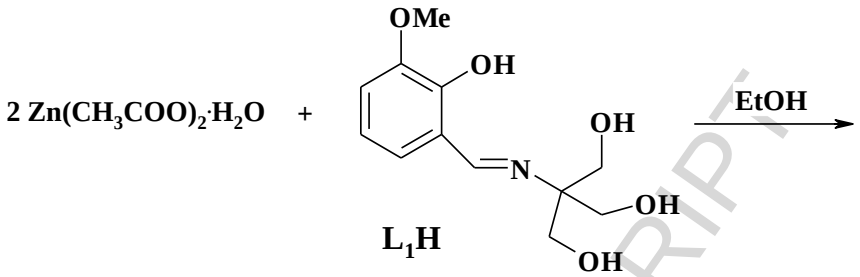

$$[Zn_2(L_1)(CH_3COO)_3] + CH_3COOH + 2\,H_2O$$

In a similar reaction, $Zn(CH_3COO)_2 \cdot 2H_2O$ reacted with Schiff base **L_2H** in ethanol. The stoichiometric reaction leading to the formation of compound $[Zn_2(L_2)(CH_3COO)_3]\cdot H_2O$ **(2)** is shown below:

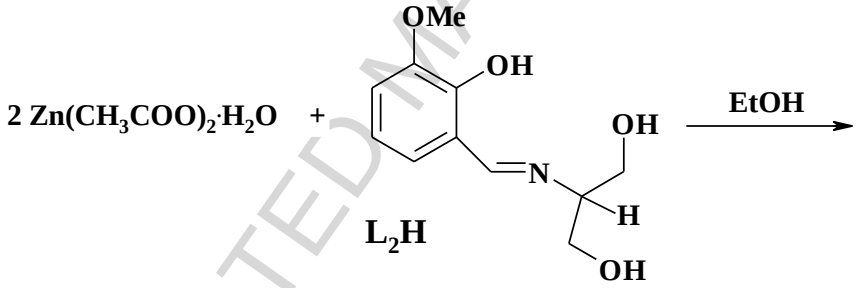

$$[Zn_2(L_2)(CH_3COO)_3] + CH_3COOH + 2\,H_2O$$

In an analogous reaction, $Zn(CH_3COO)_2 \cdot 2H_2O$ reacted with Schiff base **L_3H** in ethanol. The stoichiometric reaction leading to the formation of $Zn_2(L_3)_2(CH_3COO)_2$ **(3)** is shown below:

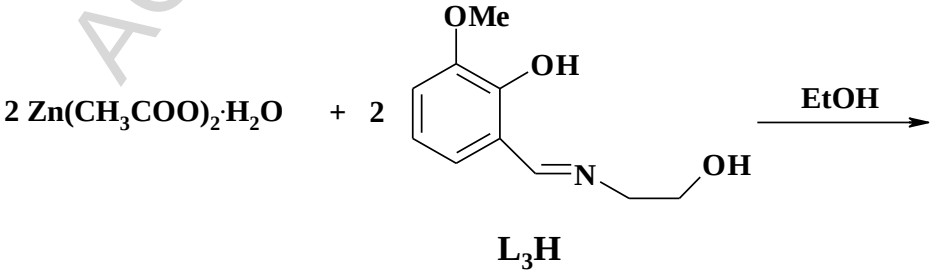

$$[Zn_2(L_3)_2(CH_3COO)_2] + 2\,CH_3COOH + 2\,H_2O$$

Diethyl ether, was added as a precipitating solvent to the reaction mixture in the first and third reactions described above. The second reaction mixture was left to evaporate slowly. Yellow crystalline materials emerged in all three reactions described above, the analytical composition of which was consistent with the formulation in **1**, **2** and **3**, respectively (*vide supra*). Positive identification of the crystalline products was achieved by elemental analysis,

ACCEPTED MANUSCRIPT

FT-IR spectroscopic methods and X-ray crystallographic determination for isolated single crystals from **1-3**. All complexes are stable in the crystalline form, in the air, for fairly long periods of time. All three freshly prepared species are readily dissolved in water and DMSO, sparingly soluble in alcohols (CH_3OH, i-PrOH), and insoluble in acetone, acetonitrile and dichloromethane at room temperature.

3.2. Description of X-ray Crystallographic Structures

The X-ray crystal structures of **1**, **2**, and **3** reveal discrete solid state lattices. The molecular structures of **1-3** are given in Figs. 1A, 2A and 3, respectively; selected bond distances and angles are listed in Table 2. The molecular structure of **1** and **2** consists of two Zn(II) ions, one $\mathbf{L}^-$ ($\mathbf{L_1}^-$, $\mathbf{L_2}^-$, respectively) and three acetato ligands, whereas the molecular structure of **3** consists of two Zn(II) ions, two $\mathbf{L}^-$ ($\mathbf{L_3}^-$) and two acetato ligands. Therefore, all three complexes **1-3** are dinuclear Zn(II) species. **1** crystallizes in the monoclinic space group $P2_1/n$, whereas **2** crystallizes in the orthorhombic space group $P2_1cn$, both with four molecules in the unit cell. In the first two complexes, the metal ions are bridged through the deprotonated phenolato oxygen atom of the **LH** ligands, which acts as a monoatomic bridge, and through two acetato ligands, which present the usual *syn,syn* bridging mode. The third acetato ligand is coordinated to one of the metal ions in an asymmetric chelating mode. All types of **L** ligands, i.e. $\mathbf{L_1}^-$, $\mathbf{L_2}^-$, $\mathbf{L_3}^-$, in **1-3** respectively, act as tetradentate chelators bound through the O_{phen}, O_{alk}, N_{imi} and O_{met} anchors. The two Zn(II) ions in **1-3** present different coordination environments. One metal ion is coordinated to the O_{phen} and O_{met} anchors of the **L** ligands and to four carboxylato oxygen atoms from the three acetate ligands, leading to a distorted octahedral geometry. The second Zn(II) ion in **1-3** is five-coordinate, bound to the O_{phen}, N_{imi} and O_{alk} anchors of the $\mathbf{L}^-$ ligands and to two carboxylato oxygen atoms from the two *syn,syn* acetato ligands. The coordination geometry of the five-coordinate metal ions is best described as a trigonal bipyramidal, based on the value of the trigonality index, τ (0.70 for **1**, 0.49 for **2**, and 0.62 for **3**). The Zn-O_{phe}, Zn-N_{imi}, Zn-$O_{acetate}$ and C-$O_{acetate}$ distances were found to be consistent with those reported in the literature [**47,48,49,50**]. A Zn-O_{met} distance of 2.385, 2.402 Å and 2.329 Å for Zn-OCH_3 binding in **1**, **2** and **3** respectively, is attributable to weak binding. It has been observed on (O,N)-bound Zn(II) complexes reported in the literature that distances in the range from 2.34 to 2.91 Å lead to highly distorted geometries [**51,52,53,54,55**]. These Zn(II)-O distances are similar to the corresponding distances in the Zn(II)-ATP complex [**51**], containing a Zn(II)-$O_{phosphato}$ distance of 2.71 Å (distorted octahedral), in Zn(II)-histidinato complexes [**52,53**], with Z(II)-$O_{carboxylato}$ distances of 2.91 and 2.79 Å (distorted octahedral), in the Zn(II)-triazacyclododecane complex [**54**],

ACCEPTED MANUSCRIPT

with Zn(II)-$O_{perchlorato}$ distances of 2.528 and 2.818 Å (distorted trigonal bipyramidal), and in the case of Zn(II)-crown ether complex [**55**], with Zn(II)-$O_{crownether}$ distances of 2.34, 2.56 and 2.60 Å. Of the three –CH_2OH groups in **1** and the two –CH_2OH groups in **2**, only one is bound to the five coordinate Zn(II) center, whereas the other –CH_2OH groups remain free. All these -OH groups are involved in hydrogen-bonding interactions in the lattice. Each molecule in the lattice of **1** interacts with four neighboring molecules via four intermolecular hydrogen bonds between the free -CH_2OH groups defined by O(3) and O(4), which act as donors and carboxylato atoms O(16) and O(13), respectively, which act as acceptors (Table 3). In doing so, the dinuclear complexes are linked to form layers extending parallel to the *ac* plane (Fig. 1B). Two neighboring layers are also linked through intermolecular hydrogen bonds between the third free -CH_2OH group defined by the disordered O(5) atom, which acts as a donor and the carboxylato atom O(16), which acts as an acceptor, thus forming double layers (Fig. 1C). In the crystal lattice of **2**, each Zn(II) complex interacts with two neighboring molecules through two intermolecular hydrogen bonds between the free -CH_2OH group defined by O(14), which acts as a donor and the carboxylato oxygen O(5), which acts as acceptor, thereby forming 1D chains parallel to the [110] crystallographic direction (Fig. 2B, Table 3). These chains form layers parallel to the (001) crystallographic plane stacked along the c-axis and further linked through intermolecular hydrogen bonds involving the lattice water molecules and the free -CH_2OH groups of the ligand. Consequently, an overall 3D network (Fig. 2C) is generated. Successive layers of chains along the c-axis are shown in magenta and blue color in Fig. 2C.

Compound **3** crystallizes in the monoclinic space group $P2_1/n$ with four independent molecules in the unit cell. In **3**, two ligands act as tetradentate and tridentate binders, respectively, the first through the O_{phen}, O_{alk}, N_{imi} and O_{met} anchors and the second through the O_{phen}, O_{alk} and N_{imi} anchors, collectively giving rise to a distorted octahedral Zn(II) center and a Zn(II) center with a distorted trigonal bipyramidal geometry (Fig. 3). The six coordinate Zn(II) center is bound to the O_{phen}, O_{alk} and N_{imi} groups of the first ligand, the O_{phen}, O_{met} terminals of the second ligand, with one coordination site being occupied by an oxygen atom of one acetato group. The five coordinate Zn(II) center is bound to the O_{phen}, O_{alk} and N_{imi} moieties of the second ligand, with two coordination sites being occupied by one carboxylato oxygen from each of the two acetato groups. One of the acetate groups acts as a bidentate bridge of the two Zn(II) centers. Two intramolecular hydrogen bond interactions occur in the lattice of **3**. The Zn(II)-bound –CH_2OH group of the six coordinate Zn(II) center is involved in a hydrogen bond interaction with the oxygen of the acetato group of the five coordinate

ACCEPTED MANUSCRIPT

Zn(II) center. The Zn(II)-bound $–CH_2OH$ group of the five coordinate Zn(II) center forms a hydrogen bond with the second oxygen of the same acetato group.

3.3. FT-IR spectroscopy. The spectra of compounds **1-3** show active ν(OH) and ν(C=N) vibrations at 3380-3439 and 1617-1644 cm^{-1}, respectively, with the binding of the imine nitrogen confirmed by lowering of the resonance frequency (13-15 cm^{-1}). Specifically, ν(OH) and ν(C=N) emerged at 3439 $cm^{-1}$and 1628 cm^{-1} for **1**, 3381 cm^{-1} and 1618 cm^{-1} for **2**, 3431 cm^{-1} and 1644 cm-1 for **3**. The ν_{asym} and ν_{sym} vibrations of the acetato groups were observed in all cases. Specifically, the antisymmetric stretching vibrations $\nu_{as}(COO^{–})$ emerged at 1595 cm^{-1} for **1**, 1562 cm^{-1} for **2**, and 1582 cm^{-1} for **3**. Symmetric stretching vibrations $\nu_{s}(COO^{–})$ for the same group appeared at 1442 cm^{-1} for **1,** 1448 $cm^{-1}$for **2,** and at 1443 cm^{-1} for **3**, with Δν being 114-153 cm^{-1}. The frequencies of the observed carbonyl vibrations were shifted to lower values in comparison to the corresponding vibrations in free acetate, indicating changes in the vibrational status of the ligands upon binding to the Zn(II) ion. All data were further confirmed by the X-ray crystal structures of **1-3**.

3.4. Solid-state NMR spectroscopy. The ^{13}C CP-MAS-NMR spectrum of **1** (Fig. 4A) was consistent with the coordination mode of the Schiff base ligand bound to Zn(II) ion. Specifically, the spectrum shows separate resonances for the various carbons of the Schiff base ligand and the acetate moiety and exhibits a distinctly different pattern compared to the free Schiff base. The resonances in the high-field region (19.6-22.6 ppm) could be assigned to the methyl groups of the variably bound acetates. The resonance at 54.3 ppm is reasonably ascribed to the methoxy group carbon atom. The signals in the range 61.0-65.7 ppm could be ascribed to the carbons of the tromethamine tether. Another group of resonances in the range 115.8-151.6 ppm could be assigned to the benzene ring of the Schiff base. In the low field region, a signal around 174.1 ppm could be assigned to the azomethine group carbon, with the broad signal around 180.7 ppm being attributable to the carboxylato group carbons of the acetates bound to Zn(II) [**56**]. The ^{13}C CP-MAS-NMR spectrum of **2** (Fig. 4B) shows resonances in the high-field region (20.5-23.1 ppm) assignable to the methyl groups of the variably bound acetates. The resonance at 53.7 ppm is reasonably ascribed to the methoxy group carbon atom. The signals in the range 59.9-77.7 ppm could be ascribed to the carbons of the aminoalcohol tether. The group of resonances in the region 116.5-152.6 ppm could be assigned to the presence of the benzene ring of the Schiff base ligand. In the low field region, a signal around 170.9 ppm could be assigned to the azomethine group carbon atom, with the broad signal around 180.1 ppm being attributable to the carboxylato group carbons of acetates bound to Zn(II). The ^{13}C CP-MAS-NMR spectrum of **3** (Fig. 4C) exhibits a distinctly

ACCEPTED MANUSCRIPT

different pattern of signals from **1** and **2**. The resonance in the high-field region (22.1 ppm) could be assigned to the methyl groups of the bound acetates. The resonance at 54.5 ppm is reasonably ascribed to the methoxy group carbon atom. The signals in the range 56.7-78.3 ppm could be ascribed to the carbons of the aminoalcohol tether. The group of resonances at 111.5-162.3 ppm could be assigned to the presence of the benzene ring in the Schiff base. In the low field region, a signal around 170.6 ppm could be assigned to the azomethine group carbon atom, with the broad signal in the range 172.8-177.7 ppm being attributable to the carboxylato group carbons of the acetates bound to Zn(II). All of the resonances appear to be shifted to slightly higher fields compared to the free ligands. These observations are consistent with the structure of the compounds revealed by X-ray crystallography.

3.5. Solution NMR spectroscopy. The solution ^{13}C-NMR spectra of freshly prepared compounds **1** and **3** were measured in D_2O. The spectrum of **1** (Fig. 5A) exhibits a) a resonance at 22.9 ppm attributed to the acetato methyl carbon, b) resonances in the range 48.0-60.8 ppm, attributed to methyl and methylene carbons, c) resonances in the range 114.5-128.3 ppm and at 150.6 ppm, attributed to the presence of aromatic carbons, d) a resonance at 170.7 ppm in agreement with the presence of the azomethine carbon of the $\mathbf{L_1}^-$ ligand bound to Zn(II) ion, and finally e) a resonance at 181.5 ppm attributed to the presence of the carboxylate carbons of the acetato ligand bound to the Zn(II) ion. The ^{13}C spectrum of **3** (Fig. 5B) exhibits a resonance at 23.2 ppm attributed to the acetato methyl carbon, b) resonances in the range 40.0-60.2 ppm, attributed to methyl and methylene carbons, and c) resonances in the range 117.1-121.8 ppm and resonance at 151.0 ppm attributed to the presence of aromatic carbons. Finally, the resonance at 181.4 ppm could be attributed to the presence of the carboxylato carbons of the acetato ligand bound to the Zn(II) ion. These observations were subsequently confirmed by X-ray crystallography. The resonance shift was ~2.0 ppm for **1** and **3** downfield and was comparable to that observed in the CP-MAS ^{13}C-NMR solid-state spectrum of **1** and **3**.

The ^{1}H-NMR spectra of **1** and **3** in D_2O showed several peaks. The spectrum of **1** (Supplementary Material Fig. S1A) exhibits resonances between 1.0-1.9 ppm. They are consistent with the presence of the methyl protons (acetato groups). The resonances between 3.2-3.6 ppm are attributed to the $–CH_2OH$ group protons. The resonance at 3.7 ppm is attributed to the methoxy group $–OCH_3$ of the $\mathbf{L_1}^-$ ligand. The resonances in the range 6.6-7.1 ppm could be attributed to the presence of aromatic protons. The resonance at 8.4 ppm could be ascribed to the proton of the –CH=N group of the $\mathbf{L_1}^-$ ligand bound to the Zn(II) ion. The spectrum of **3** (Supplementary Material Fig. S1B) exhibits resonances in the range 1.1-1.8

ACCEPTED MANUSCRIPT

ppm. They are consistent with the presence of the methyl protons (acetato groups). The resonance at 3.0 ppm is attributed to the $–CH_2OH$ group protons, the resonance at 3.6 ppm could be attributed to the $–N-CH_2$ group and the resonance at 3.7 ppm is attributed to the $–OCH_3$ group. The resonances in the range 6.6-7.1 ppm could be attributed to the presence of aromatic protons. The resonance at 8.3 ppm could be ascribed to the proton of the –CH=N group of the $\mathbf{L_3^-}$ ligand bound to Zn(II) ion.

3.6. Thermal Studies. The thermal decomposition of complexes **1-3** was studied by TGA under an atmosphere of oxygen (Fig. 6). Compound **1** is thermally stable up to 174 °C. Between 174 °C and 516 °C, there is further weight loss, in line with the decomposition of the organic structure of the molecule. No clear plateaus are reached in these stages, suggesting that the derived products are unstable and decompose further. A plateau in the decomposition of **1** is reached at 516 °C, with no further loss up to 550 °C, in line with the thesis that the product at that temperature and beyond (516 °C) is ZnO. The total weight loss of ~71.6% is in good agreement with the theoretical value ~71.0%, in line with the following tentative reactivity pattern:

$$\underset{(L_1^-)}{4\ Zn_2(C_{12}H_{16}O_5N)(CH_3COO)_3} + 79\ O_2 \longrightarrow 8\ ZnO + 72\ CO_2 + 2\ N_2 + 50\ H_2O$$

Compound **2** is thermally stable up to 60 °C. From that point on, a fairly broad heat process points to the dehydration of **2**, with the release of moisture and lattice water molecules between 60 °C and 235 °C. Between 235 °C and 490 °C, there is further weight loss, in line with the decomposition of the organic structure of the molecule. No clear plateaus are reached in these stages, suggesting that the derived products are unstable and decompose further. A plateau in the decomposition of **2** is reached at 490 °C, with no further loss up to 550 °C, in line with the thesis that the product at that temperature and beyond (490 °C) is ZnO. The total weight loss of ~70.4% is in good agreement with the theoretical value ~70.2%, in line with the following tentative reactivity pattern:

$$\underset{(L_2^-)}{4\ [Zn_2(C_{11}H_{14}O_4N)(CH_3COO)_3]\cdot H_2O} + 75\ O_2 \longrightarrow 8\ ZnO + 68\ CO_2 + 2\ N_2 + 50\ H_2O$$

Compound **3** is thermally stable up to 173 °C. Between 173 °C and 526 °C, there is further weight loss, in line with the decomposition of the organic structure of the molecule. No clear plateaus are reached in these stages, suggesting that the derived products are unstable and decompose further. A plateau in the decomposition of **3** is reached at 526 °C, with no further

ACCEPTED MANUSCRIPT

loss up to 550 °C, in line with the thesis that the product at that temperature and beyond (526 °C) is ZnO. The total weight loss of ~74.7% is in good agreement with the theoretical value ~74.2%, in line with the following tentative reactivity pattern:

$$2\ Zn_2(C_{10}H_{12}O_3N)_2(CH_3COO)_2 \ + \ 55\ O_2 \longrightarrow$$

$$4\ ZnO \ + \ 48\ CO_2 \ + \ 2\ N_2 \ + \ 30\ H_2O$$

The described tentative assignments are consistent with previously reported results of thermogravimetric analysis [**57**].

3.7. Cytotoxicity Results

3.7.1. Zn(II) toxicity in 3T3-L1 pre-adipocytes

To examine whether Zn(II) ions (non-complexed inorganic zinc) affect cell survival, 3T3-L1 pre-adipocytes were treated with 1, 10, 100 or 200 μM of either $ZnCl_2$ or $ZnSO_4$ for 24 h. Fig. **7** shows that both $ZnCl_2$ (**A**) and $ZnSO_4$ (**B**) affect cell survival in a concentration-dependent manner ($p<0.05$). Specifically, reduction in cell survival amounts to 53 % (**A**) and 50% (**B**) at 1 μM, 64 % (**A**) and 45% (**B**) at 10 μM, and 65 % (**A**) and 62% (**B**) at 100 μM, and almost 100 % at 200 μM ($p<0.05$) compared to the control. Sodium deoxycholate has been used as a positive control, exhibiting full reduction of cell survival under the employed experimental conditions.

3.7.2. Zn(II) compound toxicity in 3T3-L1 pre-adipocytes for 24h

To assess cell toxicity of Zn(II)-complexes, 3T3-L1 pre-adipocytes were treated with various concentrations (1-50 μM) of **1**-**3** for 24 h. Figs. 8A show that **3** is toxic even at low concentrations (1-50 μM) ($p<0.05$), in contrast to **2**, which is non-toxic compared to the control. Toxicity for **1** starts settling in at higher concentrations (50 μM) with the amount of cell death being ~33% ($p<0.05$). In parallel to this toxicity profiles, ligands L_1H and L_2H have been found to be non-toxic in the concentration range 1-200 μM, with ligand L_3H being toxic throughout the same range [**38**].

3.7.3. Zn(II) compound toxicity in 3T3-L1 pre-adipocytes for 48h

During induction of the differentiation process, cells are exposed to Zn(II) complexes for more than 24 h. Therefore, potential cytotoxic effects of Zn(II)-compounds were also assessed in 3T3-L1 pre- adipocytes for 48 h. Specifically, the cytotoxic effects of **1** and **2** were investigated at various concentrations (1-50 μM) ($p<0.05$) for 48 h. Figs. 8B show that both **1** and **2** appear to be non-toxic compared to the control for concentrations ranging from 1

ACCEPTED MANUSCRIPT

μM to 50 μM ($p<0.05$). It appears, therefore, that **1** and **2** can further be employed in the induction of 3T3-L1 pre-adipocyte differentiation.

3.7.4. Zn(II) compound toxicity in differentiated 3T3-L1 for 48h

To examine whether the zinc compounds affect cell survival in differentiated 3T3-L1 adipocytes, cells were treated with various concentrations (1-50 μM) of **1** and **2** for 48 h. Fig. 9 shows that both **1** and **2** appear to be non-toxic at concentrations ranging from 1 μM to 50 μM ($p<0.05$). Toxicity starts settling in at concentrations beyond 50 μM (with the exception of **1**).

3.8. Cell migration results

To assess the cell migration effect of the title compounds on 3T3-L1 pre-adipocytes, a scratch assay was performed. Cells were treated with 25 μM of each compound for 24 and 48h respectively (10x 5× magnification). The migration capacity of cells grown in the presence of only DMEM was considered as control. As shown in Fig. 10, in the case of **2** and **3**, cells exhibited decreased migration. **3** projected a complete abolishment of migration at the concentration tested, whereas **1** appeared to have no effect on cell motility as in the case of the control. Similar results were obtained after treatment for 48 h (data not shown).

3.9. In vitro insulin-like activity of Zn(II) compounds

In order to evaluate zinc's insulin-like activity, the title compounds were employed to induce cell differentiation of 3T3-L1 pre-adipocytes into mature adipocytes according to standard protocol. Both **1** and **2** induced differentiation of pre-adipocytes into mature adipocytes, as assessed by oil red O staining, in a concentration-dependent manner (0.5–50 μM). Differentiation was evident already at 1 μM and the maximal effect was observed at 25 μM (Fig. 11). This effect was comparable to the differentiation effect induced by insulin (10 ng/mL) (Fig. 11B). To further ascertain and validate the differentiation of pre-adipocytes treated with **1** and **2**, RT-PCR was run in order to determine the relative mRNA expression of PPAR-γ, GLUT 1, GLUT 3 and GLUT 4 into mature adipocytes. An increase was observed for PPAR–γ mRNA expression in mature adipocytes induced via differentiation by the title compounds compared to pre-adipocytes (Fig. 12). In the case of the constitutively expressed transporter GLUT 1, mature adipocytes differentiated with **1** and **2**, showed a significant increase in mRNA expression relative to the control, yet there was no substantial increase compared to insulin (vide infra). In the case of GLUT 3, combinations of insulin and compounds had a significant effect on its mRNA expression compared to the control. However, the combination of insulin and **1** was the only one reflecting a significant increase compared to insulin. By the same token, mature adipocytes differentiated with **1** and **2**

ACCEPTED MANUSCRIPT

showed a 3 and 4 fold increase of GLUT 4, respectively, compared to undifferentiated pre-adipocytes (Fig. 13). Interestingly, when **1** or **2** was used in combination with insulin in the differentiation medium of 3T3-L1 pre-adipocytes, a higher expression of GLUT 4 and PPAR-γ mRNA was observed in the case of **1** compared to that of insulin or **1** alone (Fig. 12 and 13C), suggesting an additive and/or synergistic effect of this compound to insulin-induced adipogenesis.

4. Discussion

4.1. The concept and emergence of ternary Zn(II)-acetato-Schiff compounds

The coordination environment of zinc modulates profusely the biological activity of that metal ion in the cellular milieu. In this respect, the nature and properties of the ligands-substrates bound into the Zn(II) coordination sphere essentially formulate the potential of that metal ion to induce phenotypic changes commensurate with the sought after effects (adipogenicity, restoration of normoglycemia, etc.). Among those ligand properties are the ultimate hydrophilic-hydrophobic character of the Zn(II) complex form, the ability to promote Zn(II) chelation through (O,N)-containing terminals and thus bring about stabilization, allowance for kinetically labile third type ligands (e.g. water) to bind the metal ion thereby setting the stage for further biological interactions of Zn(II) with cellular targets of importance to the reduction of hypergrlycemia, and others.

In view of the aforementioned, the substrates-ligands selected to explore the chemistry of Zn(II) fulfill several of the stated criteria, thus principally guiding the synthesis of ternary materials aptly poised to seek and establish interactions with molecular targets in the cellular medium linked to the insulin-like activity of fibroblast differentiation toward adipocytes, capable of reducing blood glucose levels in type 2 Diabetes mellitus. The vanillin-based Schiff ligands [**36-38**] provide a flexible cleft for Zn(II) binding through the phenolato and azomethine imino terminals, with the remaining available coordination sites being taken up by either third ligands (acetates in starting reagent) and/or the alcoholic terminals in the Schiff base. The presence of alcohols in the Schiff ligands bound to Zn(II) also provides an opportunity for establishment of interactions (i.e. through H-bonding) with intracellular molecular targets, thus promoting Zn(II) biological activity reflected in cytotoxicity, cell differentiation and/or insulin mimetic activity. In such a context, L_1H contains three amino alcoholic terminals, L_2H contains two and L_3H contains only one. Logically, therefore, the synthetic approaches used in this work are linked to a common source of Zn(II) a) as a synthon containing bound acetato groups, and b) under appropriate reaction conditions ensuring the isolation of dinuclear assemblies bearing the appropriate components (ligands

ACCEPTED MANUSCRIPT

and acetato groups) and carrying newly formulated chemical properties bestowed upon the Zn(II) assemblies. The physicochemical characterization of the ligands and the associated materials **1**-**3** relying on elemental analysis, FT-IR, ESI-MS, NMR and X-ray crystallography confirm their nature, thereby justifying their further use in biological experiments.

4.2. Structure-based association with potential Zn(II) biological activity

The isolated ternary Zn(II) compounds **1**-**3** are chemically well-defined species, which owing to their design and synthetic emergence are poised to seek biological activity at the molecular level. To this end, the three materials belong to a uniform family of species, with common features including the following: a) they are dinuclear complexes of Zn(II), b) they all contain at least one Schiff ligand (compound **3** contains 2 ligands) bound to Zn(II), c) they all contain acetato groups bound to Zn(II), and d) in all three compounds the Schiff ligand is singly deprotonated, with the amino alcoholic moieties retaining their protons.

Specifically, in **1**, two of the acetato ligands span over the two Zn(II) ions in the dinuclear assembly with the third acetato ligand coordinating one of the two Zn(II) centers in a bidentate fashion. That ligand coordination activity around the dinuclear assembly generates an organizational asymmetry in the molecule, with the tri-alcoholic tether extending on one end only. In this sense, it's worth emphasizing the fact that one of the three amino alcoholic moieties in the dinuclear assembly binds a Zn(II), while still retaining its alcoholic proton, with the other two dangling away from the Zn(II) core. This apparent structural arrangement might have implications on the exertion of biological behavior of the compound. In **2**, the same motif of acetato groups bound to the dinuclear assembly is recognized as in **1**, with the di-alcoholic moiety attached to the Schiff core dangling away from the dinuclear assembly and only one alcoholic moiety remaining protonated and bound to one Zn(II) center. The so arising asymmetry in the ligand arrangements around the dinuclear core resembles that encountered in **1**. Worth noting at this juncture is the fact that **1**, containing Zn(II) bound to L_1^-, emerges as toxic as the free ligand L_1H itself, in stark contrast to the congener vanadium compound bearing the same ligand bound to V(V). The latter species was not toxic to the cells [**38**].

In **3**, one of the acetato groups spanning the dinuclear Zn(II) unit has been replaced by a second Schiff ligand bound to the unit, thereby raising the number of bound Schiff ligands to two. The terminally bound acetato group to one of the Zn(II) centers differentiates itself from the corresponding ones in **1** and **2** in that it binds the metal ion center in a monodentate fashion. The so arranged ligands in the dinuclear core introduce an asymmetric character in the molecule, reflected ostensibly in the structural features inherent to the Zn(II) core.

ACCEPTED MANUSCRIPT

The aforementioned description of the three molecules reveals differences among the species that include the following: a) a variable number of coordinated acetato groups to the dinuclear Zn(II) assemblies (three for **1** and **2** and two for **3**), b) a variable coordination mode in the terminally bound acetato groups to the Zn(II) dinuclear core, b) a variable Zn(II):Schiff base ligand ratio (2:1 for **1** and **2** and 1:1 for **3**) in the dinuclear assemblies, and c) a variable number of amino alcoholic tethers, thereby projecting potentially differing-variable capacities in the pursuit of interactions (i.e. hydrogen bonding) with cellular targets. Collectively, the outlined similarities and differences in **1**-**3** signify some of the factors that might influence the activity of the three species at the biological level in terms of toxicity and cellular differentiation related to insulin mimetic activity toward fibroblast differentiation (vide infra). In this sense, the biological profiles of **1**-**3** arising in the experiments could further be amenable to optimization of the observed biological activity of Zn(II) through adjustments in the nature and properties of the ligands seeking metal ion coordination and leading to dinuclear Zn(II) assemblies.

4.3. Structure-selective influence of Zn(II)-compounds on pre- and mature adipocyte survival.

Diabetes mellitus is a group of metabolic diseases mainly characterized by disregulation of glucose metabolism. There is a significant correlation between zinc and Diabetes mellitus, although an intricate bilateral web of complex interactions still remains unclear. Zinc can directly affect insulin secretion, synthesis and signaling. In this respect, the present work examined the insulin-like effect of three newly synthesized zinc compounds toward induction of pre-adipocyte cell differentiation. The results, clearly demonstrate the differentiating potential of zinc complexes. Zn(II) ions (from $ZnCl_2$ or $ZnSO_4$) appear to reduce cell viability in a concentration-dependent manner. The cytotoxic effects of zinc ions are reduced through complexation. Consequently, the nature of substrates to which Zn(II) is bound *does emerge* crucial to the biological activity it exemplifies. In fact, the results indicate the structure-specific influence of (L_1^-)-(L_3^-) Zn(II)-bound ligands on pre-adipocyte survival. Hence, the toxicity profile exemplified by the Zn(II)-L_i (i=1-3) compounds mirrors that of the free ligands. **1** and **2** appear to be non-toxic, whereas **3** influences cell survival in a concentration-dependent manner. Interestingly, the emerging cytotoxic pattern, when pre-adipocytes were treated with **3** for 24 h, is almost the same as that of the substrate (L_3H) to which zinc is ligated. In addition, the cytotoxic profile of each compound examined clearly depends on the number of terminal alcohol arms. Along the same lines, a cell migration test was performed on each zinc compound with the specific cell line. To this end, it's worth

ACCEPTED MANUSCRIPT

noting the fact that the specific cell line exemplifies chemotactically its cell migration potential. The results reveal that although a zinc compound can be non-toxic, it may have an effect on the endogenous cell motility. The overall results indicate that **1** does not affect cell migration following 24 h treatment as in the case of the control.

4.4. Zinc-induced adipogenesis with insulin-like activity

The adipogenic effect of insulin is one of the most fundamental functions of insulin signaling in adipose tissue and depends on several signaling molecules, including insulin receptor substrate 1 and 2, phosphoinositide 3-kinase, and protein kinase B. The murine 3T3-L1 cell is an established insulin-responsive pre-adipocyte model for the study of adipogenesis. As a result, this cell line is used in order to investigate the differentiation potential of **1** and **2.** Both compounds induced differentiation of pre-adipocytes into mature adipocytes in a concentration-dependent manner similar to the effect induced by insulin, thereby demonstrating the adipogenic potential of the title compounds. Increased expression of peroxisome proliferator activated receptor gamma (PPAR-γ) and glucose transporter 4 (GLUT 4) in mature adipocytes treated with the Zn(II) compounds further confirmed the differentiation capacity of these complexes. Increased expression of PPAR-γ a) is an early event during differentiation of an adipocyte precursor cell toward a fully mature adipocyte, and b) induces the expression of late-stage-differentiation genes. In turn, once a cell is transformed into a mature adipocyte, glucose transporters belonging to the GLUT family emerge as significant players in glucose metabolism. In this respect, the employment of three members of that family, i.e. GLUT 1, GLUT 3 and GLUT 4, arose as a key subject of this investigation related to biomarker-driven proof of the cell differentiation process having taken place. To this end, in the case of GLUT 1, compounds 1 and 2 fared a) at almost the same level of mRNA expression as insulin, and b) marginally above the untreated pre-adipocytes (control). The combination of **1** and **2** with insulin did not result in any substantially higher mRNA expression levels compared to the control either. The collective results a) are in line with literature reports on GLUT 1 mRNA levels expressed at a basal level, essentially not changing between pre- and mature adipocytes [**58**], and b) suggest that the title zinc compounds **1** and **2** do not influence the expression of constitutive components (such as GLUT 1) in glucose uptake. In GLUT 3, the pattern of mRNA expression in the case of insulin and combinations thereof with **1** and **2** is similar to that of GLUT 4 (vide infra), thereby indicating that the title compounds **1** and **2** can stimulate mRNA expression of glucose transporters intimately associated with targets expressed mainly in non tissue-specific cells (i.e. neuronal) [**59**,**60**]. The overall fold increase of the relative mRNA concentration of

ACCEPTED MANUSCRIPT

GLUT 1 is lower than two-fold compared to the control, thus ascertaining its constitutive role in adipocyte physiology [**61**]. Concomitantly, GLUT-4 plays a major role in the metabolic functions of adipocytes by allowing glucose transport into the cell during stimulation by insulin. It is the main glucose transporter specific for adipose tissues and 3T3-L1 cell line [**62**,**63**]. To this end, basal levels of GLUT 4 project a reliable biomarker for cell adipogenesis. Glucose transport occurs relatively late in the differentiation process following expression of PPAR-γ. Increased expression of PPAR-γ in adipose tissue results in rising levels of GLUT-4 [**64**]. Inhibition of adipogenesis results in decreased expression of both PPAR-γ and GLUT-4 [**65**]. The greater increase in the expression of GLUT 4 and PPAR-γ observed upon combinational treatment of pre-adipocytes with insulin and Zn(II)-compounds compared to insulin, and Zn(II)-compounds alone, indicates a possible additive and/or synergistic effect between the two agents. Such insulin-like effects may involve zinc potentiation of insulin signal transduction pathways, and/or enhancement of insulin action through Zn(II)-compound interjection, thereby contributing to a significantly greater increase in the expression of adipogenesis molecular factors.

5. Conclusions

The work presented here a) projects the benefits of ligand L_iH (i=1-3) design exemplifying the salient structural and electronic characteristics of ternary Zn(II)-L-acetato species **1**-**3** as potential adipocyte differentiating agents mimicking insulin, b) delineates the crystallographic and spectroscopic properties of the arising materials **1**-**3** through the elaborated synthetic procedures adopted, and c) describes the biological effects brought on by the use of structure-based selection of synthetic zinc forms in biological tests linked to insulin action on pre- and mature adipocytes. Ligand structural differentiation exemplified through the variable number of alcohol-containing "arms"-anchors in the Schiff base(s) employed, variably configuring the nature of the arising Zn(II) species, suggests an association of the Zn(II)-bound ligand to cellular toxicity and concomitant biological activity. The experimental account delves into the biological effects associating Zn(II) with insulin-like adipogenesis. The collective results reflect associations of properly configured and structurally selected "zincoforms" with well-defined biological profiles and set the stage for further physicochemically-based development of efficient zinc antidiabetic metallodrugs.

Appendix A. Supplementary data

Supplementary NMR data on **1** and **3** in the form of figures were deposited as Supplementary Material (Figs. S1A-B). CCDC 1059871 (**1**), CCDC 1059872 (**2**), and CCDC 1059870 (**3**) contain the supplementary crystallographic data for this paper. These data can be obtained

ACCEPTED MANUSCRIPT

free of charge via www.ccdc.cam.ac.uk/conts/retrieving.html (or from the Cambridge Crystallographic Data Centre, 12 Union Road, Cambridge CB21EZ, UK; fax: (+44) 1223-336-033; or deposit@ccde.cam.ac.uk).

Abbreviation list

DM	Diabetes mellitus
IRSs	Insulin receptor substrates
PI3K	Phosphatidylinositol 3-kinase
GLUTs	Glucose transporters
PTP1B	Protein tyrosine phosphatase B
DMSO	Dimethyl sulfoxide
DMEM	Dulbecco's modified Eagle's medium
PPAR-γ	Peroxisome proliferator-activated receptor gamma
EtOH	Ethanol
FBS	Fetal Bovine Serum
SEM	Standard error mean
ANOVA	One way analysis of variance

ACCEPTED MANUSCRIPT

ACCEPTED MANUSCRIPT

References

[**1**] J.B. Classen, Evidence childhood epidemics of type 1 and type 2 diabetes are opposite extremes of an immune spectrum disorder induced by immune stimulants. Role of race and associated cortisol activity as a major determining factor of the type of diabetes, Diabetes & Metabolic Syndrome: Clinical Research & Reviews (2008)

[**2**] S.E. Khan, Diabetologia 46 (2003) 3–19.

[**3**] H. Yki-Järvinen, Diabetologia 38 (1995) 1378–88.

[**4**] A. Gastaldelli, E. Ferrannini, Y. Miyazaki, M. Matsuda, RA. DeFronzo, Diabetologia 47 (2004) 31-9.

[**5**] E. Ferrannini, A. Mari, Diabetologia 47 (2004) 943-56.

[**6**] L. Monnier, C. Colette, D.R. Owens, Diabetes & Metabolism 34 (2008) 207-216.

[7] H. Sakurai, A. Katoh, Y. Yoshikawa, Bull. Chem. Soc. Jpn. 79 (2006) 1645–1664.

[8] B.L. Vallee, K.H. Falchuk, Physiol. Rev. 73 (1993) 79–118.

[**9**] N. Wellinghausen, H. Kirchner, L. Rink, Immunol. Today 18 (1997) 519–521.

[**10**] A.S. Prasad, Nutrition 11 (1995) 93–9.

[**11**] A.B. Chausmer, J. Am. Coll. Nutr. 7 (1998) 109–115.

[**12**] A.Q. Truong-Tran, LH. Ho, F. Chai, PD. Zalewski, J. Nutr. 130 (2000) 1459S–1466S.

[**13**] A.Q. Truong-Tran, J. Carter, RE. Ruffin, PD. Zalewski, Biometals 14 (2001) 315–330.

[**14**] H. Haase, E. Mocchegiani, L. Rink, Biogerontology 7 (2006) 421–428.

[**15**] D.A. Scott, Biochem. J. 28(4) (1934) 1592–1602.

[**16**] S.F. Simon, C.G. Taylor, Exp. Biol. Med. 226 (2001) 43.

[**17**] M.M. James, S.C. Charles, J. Biol. Chem. 257 (1982) 4362.

[**18**] H. Sakurai, Y. Kojima, Y. Yoshikawa, K. Kawabe, H. Yasui, Coord. Chem. Rev. 26 (2002) 187.

[**19**] C.G. Taylor, BioMetals 18 (2005) 305.

[**20**] L. Coulson, P. Dandona, Diabetes 29 (1980) 665.

[**21**] A. Shisheva, D. Gefel, Y. Shechter, Diabetes 41 (1992) 982.

[**22**] M.D. Chen, S.J. Liou, P.Y. Lin, V.C. Yang, P.S. Alexander, Biol. Trace Elem. Res. 61 (1998) 303.

[**23**] J. Fugono, K. Fujimoto, H. Yasui, K. Kawabe, Y. Yoshikawa, Y. Kojima, H. Sakurai, Drug Metab. Pharmacokinet. 17 (2002) 340.

[**24**] H. Sakurai, Y. Adachi, BioMetals 18 (2005) 319.

ACCEPTED MANUSCRIPT

[25] R.R. Holman, C.A. Cull, R.C. Turner, Diabetes Care 22(6) (1999) 960–964.

[26] S. Patai, The Chemistry of the Carbon-Nitrogen Double Bond, J. Wiley & Sons, London (1970).

[27] E. Jungreis, S. Thabet, Analytical Applications of Schiff bases, Marcell Dekker, New York (1969).

[28] D.H. Brown, W.E. Smith, Enzyme Chemistry- impact and Applications, Chapman and Hall, London (1990).

[29] A.L. Lehninger, Principles of Biochemistry, Worth, New York (1975).

[30] M.B. Ferrari, S. Capacchi, G. Pelosi, G. Reffo, P. Tarasconi, R. Albertini, S. Pinelli, P. Lunghi, Inorg. Chim. Acta 286 (1999) 134.

[31] E. Canpolat, M. Kaya, J. Coord. Chem. 57 (2004) 1217.

[32] M. Yildiz, B. Dulger, S.Y. Koyuncu, B.M. Yapici, J. Indian Chem. Soc. 81 (2004) 7.

[33] K. Singh, M.S. Barwa, P. Tyagi, Eur. J. Med. Chem. 42 (2007) 394.

[34] P.G. Cozzi, Chem. Soc. Rev. 33 (2004) 410.

[35] S. Chandra, J. Sangeetika, J. Indian Chem. Soc. 81 (2004) 203.

[36] M. Odabaşoğlu, C. Albayrak, O. Büyükgüngör, P. Lönnecke, Acta Cryst. C59 (2003) o616-o619.

[37] G.X. Tana, X.C. Liub, Acta Cryst. E65 (2009) o559.

[38] E. Halevas, O. Tsave, M. P. Yavropoulou, A. Hatzidimitriou, J. G. Yovos, V. Psycharis, C. Gabriel, A. Salifoglou, Inorg. Biochem. (2015) in press.

[39] Rigaku/MSC (2005). *CrystalClear*. Rigaku/MSC Inc., The Woodlands, Texas, USA.

[40] (a) Sheldrick, G.M., SHELXS-97: Structure Solving Program, University of Göttingen, Germany, 1997. (b) Sheldrick, G.M., SHELXL-97: Crystal Structure Refinement Program, University of Göttingen, Germany, 1997.

[41] Bruker Analytical X-ray Systems, Inc. Apex2, Version 2 User Manual, M86-E01078, Madison, WI, 2006.

[42] Siemens Industrial Automation, Inc. SADABS: Area-Detector Absorption Correction; Madison, WI, 1996.

[43] Palatinus, L.; Chapuis, G. J. Appl. Cryst. 40 (2007) 786-790.

[44] P.W. Betteridge, J.R. Carruthers, R.I. Cooper, K. Prout, D.J. Watkin, J. Appl. Cryst. 36 (2003) 1487.

[45] DIAMOND – Crystal and Molecular Structure Visualization, Ver. 3.1c, Crystal Impact, Bonn, Germany, 2006.

ACCEPTED MANUSCRIPT

[46] L. Madsen, R. K. Petersen, M. B. Sörensen, C. Jörgensen, P. Hallenborg, L. Pridal, J. Fleckner, E.-Z. Amri, P. Krieg, G. Furstenberger, R. K. Berge, K. Kristiansen Biochem. J. 375 (2003) 539–549.

[47] G.B. Deacon, R.J. Phillips, Coordin. Chem. Rev. 33 (1980) 227.

[48] C.O. Rodriguez, C.O.R. de Barbarin, N.A. Bailey, D.E. Fenton, Q.Y. He, J. Chem. Soc., Dalton Trans. (1997) 161.

[49] A. Erxleben, J. Hermann, J. Chem. Soc., Dalton Trans. (2000) 569.

[50] A. Abufarag, H. Vahrenkamp, Inorg. Chem. 34 (1995) 2207.

[51] P. Orioli, R. Cini, D. Donati, S. Mangani, J. Am. Chem. Soc. 103 (1981) 4446.

[52] M.M. Harding, S.J. Cole, Acta Crystallogr. 16 (1963) 643.

[53] R.H. Kretsinger, F.A. Cotton, R.F. Bryan, Acta Crystallogr. 16 (1963) 651.

[54] S.C. Rawle, A.J. Clarke, P. Moore, N.W. Alcock, J. Chem. Soc., Dalton Trans. (1992) 2755.

[55] A.B. Charette, J.-F. Marcoux, F. Bélanger-Gariépy, J. Am. Chem. Soc. 118 (1996) 6792.

[56] C.P. Rao, A. Sreedhara, P.V. Rao, M.B. Verghese, K. Rissanen, E. Kolehmainen, N.K. Lokanath, M.A. Sridhar, J.S. Prasad, J. Chem. Soc., Dalton Trans., (1998) 2383-2393.

[57] C. Duval, "Inorganic Thermogravimetric Analysis", Second and Revised Edition, Elsevier Publishing Co., Amsterdam, (1963) 294-300.

[58] S. Perrini, L. Laviola, A. Cignarelli, M. Melchiorre, F. De Stefano, C. Caccioppoli, A. Natalicchio, M. R. Orlando, G. Garruti, M. De Fazio, G. Catalano, V. Memeo, R. Giorgino, F. Giorgino, Diabetologia 51 (2008) 155–164.

[59] T. Kayano, H. Kuomoto, T. Eddy, Y.-S. Fan, M.G. Byers, T.B. Shows, G.I. Bell, J. Biol. Chem. 263 (1988) 12245-12248.

[60] Guillet-Deniau, A. Leturque, J. Girard, J. Cell Sci. 107 (1994) 487-496.

[61] M. Mueckler, Diabetes 39 (1990) 6-11.

[62] S.W. Cushman, L.J. Wardzala, J. Biol. Chem. 255, (1980) 4758-4762.

[63] K. Suzuki, T. Kono, Proc. Natl. Acad. Sci. U.S.A. 77 (1980) 2542-2545.

[64] E.D. Rosen, B.M. Spiegelman, J. Biol. Chem. 276 (2001) 37731–37734.

[65] T. Furuyashiki, H. Nagayasu, Y. Aoki, H. Bessho, T. Hashimoto, K. Kanazawa, H. Ashida, Biosci. Biotechnol. Biochem. 68 (2004) 2353–2359.

ACCEPTED MANUSCRIPT

Table 1: Summary of Crystal, Intensity Collection and Refinement Data for $[Zn_2(L_1)(CH_3COO)_3]$ (**1**), $[Zn_2(L_2)(CH_3COO)_3]\cdot H_2O$ (**2**) and $[Zn_2(L_3)_2(CH_3COO)_2]$ (**3**).

	1	**2**	**3**
formula	$C_{18}H_{25}NO_{11}Zn_2$	$C_{17}H_{25}NO_{11}Zn_2$	$C_{24}H_{30}N_2O_{10}Zn_2$
molecular mass	562.13	550.12	637.27
T, ^oK	160(2)	160(2)	295(2)
radiation type	Cu K_α	Cu K_α	Mo K_α
wavelength, λ (Å)	1.54178	1.54178	0.71073
crystal system	monoclinic	orthorhombic	monoclinic
space group	$P2_1/n$	$P2_1cn$	$P2_1/n$
a (Å)	8.8477(2)	7.7448(1)	12.1435(11)
b (Å)	25.5944(5)	13.7545(2)	15.7193(16)
c (Å)	9.9881(2)	20.0501(3)	14.174(2)
α, deg	90	90	90
β, deg	109.496(1)	90	97.797(4)
γ, deg	90	90	90
V, ($Å^3$)	2132.14(8)	2135.85(5)	2680.6(5)
Z	4	4	4
D_{calcd} (Mg m^{-3})	1.751	1.711	1.579
abs.coeff. (μ), mm^{-1}	3.327	3.304	1.847
range of h,k,l	-10→10, -22→28, -11→11	-9→9, -16→16, -22→19	-15→16, -19→21, -19→18
goodness-of-fit on F^2	1.084	1.052	1.000
observed reflections ($I>2\sigma(I)$)	3471	3454	3666

ACCEPTED MANUSCRIPT

R [(1)]	0.0311[(1)]	0.0286[(1)]	0.0349[(2)]
R_w[(1)]	0.0769[(1)]	0.0737[(1)]	0.0662[(2)]

(1) R values are based on F values, R_w values are based on F^2; $w = 1/[\sigma^2(F_o^2) + (aP)^2 + bP]$ where $P = (\text{Max}(F_o^2, 0) + 2F_c^2)/3$

$$R = \frac{\sum \| |F_o| - |F_c| \|}{\sum (|F_o|)}, \quad R_w = \sqrt{\sum \left[w(F_o^2 - F_c^2)^2 \right] / \sum \left[w(F_o^2)^2 \right]}$$

(2) $w' \times [1 - (\Delta F_{obs} / 6 \times \Delta F_{est})^2]^2$

$w' = [P_0 T_0'(x) + P_1 T_1'(x) + \ldots P_{n-1} T_{n-1}'(x)]^{-1}$, where P_i are the coefficients of a Chebychev series in $t_i(x)$, and $x = F_{calc}^2 / F_{calc}^2{}_{max}$. P_0 - P_{n-1} =1.40 1.63 0.374

ACCEPTED MANUSCRIPT

ACCEPTED MANUSCRIPT

Table 2: Bond lengths [Å] and angles [deg] for for $[Zn_2(L_1)(CH_3COO)_3]$ (**1**), $[Zn_2(L_2)(CH_3COO)_3]\cdot H_2O$ (**2**) and $[Zn_2(L_3)_2(CH_3COO)_2]$ (**3**).

1		**2**		**3**	
Bond lengths (Å)					
Zn(1)—O(1)	2.385(2)	Zn(1)—O(1)	1.978(2)	Zn(1)—O(1)	2.329(2)
Zn(1)—O(2)	1.970(2)	Zn(1)—O(3)	1.960(2)	Zn(1)—O(2)	2.011(2)
Zn(1)—O(11)	2.009(2)	Zn(1)—O(12)	2.043(2)	Zn(1)—N(2)	2.035(3)
Zn(1)—O(13)	2.053(2)	Zn(1)—O(13)	2.163(2)	Zn(1)—O(4)	1.984(2)
Zn(1)—O(15)	2.001(2)	Zn(1)—N	2.051(2)	Zn(1)—O(5)	2.310(3)
Zn(1)—O(16)	2.497(2)	Zn(2)—O(2)	2.026(2)	Zn(1)—O(7)	2.068(3)
Zn(2)—N(1)	2.030(2)	Zn(2)—O(4)	2.041(2)	Zn(2)—N(1)	2.001(3)
Zn(2)—O(2)	2.035(2)	Zn(2)—O(5)	2.030(2)	Zn(2)—O(2)	2.065(2)
Zn(2)—O(3)	2.157(2)	Zn(2)—O(6)	2.339(2)	Zn(2)—O(3)	2.252(3)
Zn(2)—O(12)	1.955(2)	Zn(2)—O(11)	2.402(2)	Zn(2)—O(8)	1.937(2)
Zn(2)—O(14)	1.985(2)	Zn(2)—O(12)	1.987(2)	Zn(2)—O(9)	1.988(3)
Bond angles (deg)					
O(1)—Zn(1)—O(2)	72.86(7)	O(1)—Zn(1)—O(3)	107.30(9)	N(2)—Zn(1)—O(1)	93.55(11)
O(1)—Zn(1)—O(11)	159.08(7)	O(1)—Zn(1)—O(12)	95.45(9)	N(2)—Zn(1)—O(2)	156.68(11)
O(1)—Zn(1)—O(13)	98.22(7)	O(1)—Zn(1)—O(13)	90.14(10)	O(1)—Zn(1)—O(2)	73.58(9)
O(1)—Zn(1)—O(15)	85.48(6)	O(1)—Zn(1)—N	133.17(9)	N(2)—Zn(1)—O(4)	91.47(11)
O(1)—Zn(1)—O(16)	78.37(6)	O(3)—Zn(1)—O(12)	102.21(9)	O(1)—Zn(1)—O(4)	86.51(11)
O(2)—Zn(1)—O(11)	97.20(7)	O(3)—Zn(1)—O(13)	92.08(10)	O(2)—Zn(1)—O(4)	106.70(10)
O(2)—Zn(1)—O(13)	98.28(7)	O(3)—Zn(1)—N	118.01(10)	N(2)—Zn(1)—O(5)	74.87(11)
O(2)—Zn(1)—O(15)	154.30(7)	O(12)—Zn(1)—O(13)	162.28(9)	O(1)—Zn(1)—O(5)	80.60(11)
O(2)—Zn(1)—O(16)	103.72(6)	O(12)—Zn(1)—N	86.45(9)	O(2)—Zn(1)—O(5)	83.73(10)

ACCEPTED MANUSCRIPT

O(11)—Zn(1)—O(13)	101.46(7)	O(13)—Zn(1)—N	77.53(10)	O(4)—Zn(1)—O(5)	160.47(11)
O(11)—Zn(1)—O(15)	98.52(7)	O(2)—Zn(2)—O(4)	98.08(10)	N(2)—Zn(1)—O(7)	99.00(12)
O(11)—Zn(1)—O(16)	86.52(7)	O(2)—Zn(2)—O(5)	99.93(10)	O(1)—Zn(1)—O(7)	166.50(10)
O(13)—Zn(1)—O(15)	98.36(7)	O(2)—Zn(2)—O(6)	158.34(9)	O(2)—Zn(1)—O(7)	92.92(10)
O(13)—Zn(1)—O(16)	155.48(7)	O(2)—Zn(2)—O(11)	95.51(10)	O(4)—Zn(1)—O(7)	98.06(13)
O(15)—Zn(1)—O(16)	57.31(7)	O(2)—Zn(2)—O(12)	95.70(9)	O(5)—Zn(1)—O(7)	97.84(13)
N(1)—Zn(2)—O(2)	89.56(7)	O(4)—Zn(2)—O(5)	95.58(9)	N(1)—Zn(2)—O(2)	88.89(10)
N(1)—Zn(2)—O(3)	77.81(7)	O(4)—Zn(2)—O(6)	91.98(9)	N(1)—Zn(2)—O(3)	78.23(11)
N(1)—Zn(2)—O(12)	122.37(8)	O(4)—Zn(2)—O(11)	165.00(11)	O(2)—Zn(2)—O(3)	166.22(10)
N(1)—Zn(2)—O(14)	125.10(8)	O(4)—Zn(2)—O(12)	99.13(9)	N(1)—Zn(2)—O(8)	117.67(12)
O(2)—Zn(2)—O(3)	167.36(6)	O(5)—Zn(2)—O(6)	59.81(9)	O(2)—Zn(2)—O(8)	101.23(10)
O(2)—Zn(2)—O(12)	99.28(7)	O(5)—Zn(2)—O(11)	88.41(7)	O(3)—Zn(2)—O(8)	89.24(10)
O(2)—Zn(2)—O(14)	95.66(7)	O(5)—Zn(2)—O(12)	156.79(9)	N(1)—Zn(2)—O(9)	129.04(12)
O(3)—Zn(2)—O(12)	87.20(7)	O(6)—Zn(2)—O(11)	77.52(9)	O(2)—Zn(2)—O(9)	94.01(10)
O(3)—Zn(2)—O(14)	92.14(7)	O(6)—Zn(2)—O(12)	101.65(9)	O(3)—Zn(2)—O(9)	90.37(11)
O(12)—Zn(2)—O(14)	110.60(8)	O(11)—Zn(2)—O(12)	73.02(8)	O(8)—Zn(2)—O(9)	111.56(12)

ACCEPTED MANUSCRIPT

Table 3. Hydrogen bonds in **1-3**

Interaction	D···A (Å)	H···A (Å)	D-H···A (°)	Symmetry operation
		1		
O(3)-H(3O)···O(16)	2.706	1.928	167.7	-1+x, y, z
O(4)-H(4O)···O(13)	2.874	2.165	162.9	x, y, 1+z
O(5)···O(16)[a]	2.955			-0.5+x, 0.5-y, 0.5+z
		2		
O(13)-H(13O)···O(1w)	2.632	1.812	161.6	x, y, z
O(14)-H(14O)···O(5)	2.662	1.981	177.1	0.5+x, -0.5+y, 1.5-z
O(1w)-H(1wA)···O(14)	2.835	1.996	166.7	-1+x, y, z
O(1w)-H(1wB)···O(14)	2.764	1.916	174.9	-0.5+x, 1-y, 1-z

[a] O(5) was found disordered over two positions; therefore, no hydrogen atoms were included in the refinement.

		3		
O(3) – H(31)··· O(10)	2.586(6)	1.785	169.06(13)	x, y, z
O(5) – H(51)···O(9)	2.641(6)	1.839	162.99(14)	x, y, z

ACCEPTED MANUSCRIPT

ACCEPTED MANUSCRIPT

Figure Captions

Fig. 1: **(A)** Labeled plot of **1**. Hydrogen atoms (except for terminal alcohol moieties) were omitted for clarity. Color code: Zn, light blue; O, red; N, blue; C, grey; H, green. **(B)** A small part of the 2D layer in **1** due to hydrogen bonding interactions (yellow lines). **(C)** A small part of the double layers in **1** due to hydrogen bonding interactions (see text for details). Color code: Zn, deep purple; O, red; N, blue; C, grey.

Fig. 2: **(A)** Labeled plot of **2**. Hydrogen atoms (except for terminal alcohol moieties) were omitted for clarity. Color code: Zn, light blue; O, red; N, blue; C, grey; H, green. **(B)** Side and parallel views of a small part of the 1D chains along the (110) crystallographic direction in **2** due to hydrogen bonding interactions (light green dashed lines). **(C)** Successive layers of chains indicated with magenta and blue colors and stacked along the **c**-axis; the oxygen atoms of lattice water molecules are shown as red spheres and their hydrogen bonds to oxygen atoms of neighboring chains as orange lines. Color code: Zn, deep purple; O, red; N, blue; C, grey.

Fig. 3: Labeled plot of **3**. Hydrogen atoms (except for terminal alcohol moieties) were omitted for clarity. Color code: Zn, light blue; O, red; N, blue; C, grey; H, green.

Fig. 4: ^{13}C-CPMAS NMR of **1** (**A**), **2** (**B**), and **3** (**C**).

Fig. 5: ^{13}C-NMR of **1** (**A**), and **3** (**B**) in D_2O.

Fig. 6: TGA diagrams of **1** (**A**), **2** (**B**), and **3** (**C**).

Fig. 7: Percent change of cell survival in 3T3-L1 pre-adipocytes following treatment with various concentrations (1-200 μM) of either $ZnCl_2$ (**A**) or $ZnSO_4$ (**B**) for 24 h. Sodium deoxycholate has been used as a positive control. Values represent the mean value of several (no less than triplicate) independent experiments. Vertical bars represent SEMs. *: $p < 0.05$ vs. control.

ACCEPTED MANUSCRIPT

Fig. 8: Percent change of cell survival in 3T3-L1 pre-adipocytes following treatment with various concentrations (1-50 μM) of **1**, **2** and **3** for 24 h (**A**) and **1** and **2** for 48 h (**B**). Sodium deoxycholate has been used as a positive control. Values represent the mean value of several (no less than triplicate) independent experiments. Vertical bars represent SEMs.*: $p < 0.05$ vs. control.

Fig. 9: Percent change of cell survival in 3T3-L1 mature adipocytes following treatment with various concentrations (1-50 μM) of **1** and **2** for 48 h. Sodium deoxycholate has been used as a positive control. Values represent the mean value of several (no less than triplicate) independent experiments. Vertical bars represent SEMs. *: $p < 0.05$ vs. control.

Fig. 10: Cell migration of 3T3-L1 **A**) control (t=0), **B** and **C)** control after 24 h, **D**) cells treated with 25 μM of **1**, **E**) cells treated with 25 μM of **2**, and **F**) cells treated with 25 μM of **3**, using a standard scratch assay.

Fig. 11: Differentiation of 3T3-L1 pre-adipocytes (**A**) into mature adipocytes assessed by Oil red O staining following treatment with (**B**) insulin 10 ng/mL, (**C**) **2** (25 μM), and (**D**) **1** (25 μM).

Fig. 12: Relative concentration of mRNA expression for PPAR-γ in mature adipocytes treated with insulin or zinc compounds compared to pre-adipocytes ($p<0.05$).

Fig. 13: Relative concentration of mRNA expression for GLUT 1 (**A**), GLUT 3 (**B**), and GLUT 4 (**C**) in mature adipocytes treated with insulin or zinc compounds compared to pre-adipocytes ($p<0.05$).

ACCEPTED MANUSCRIPT

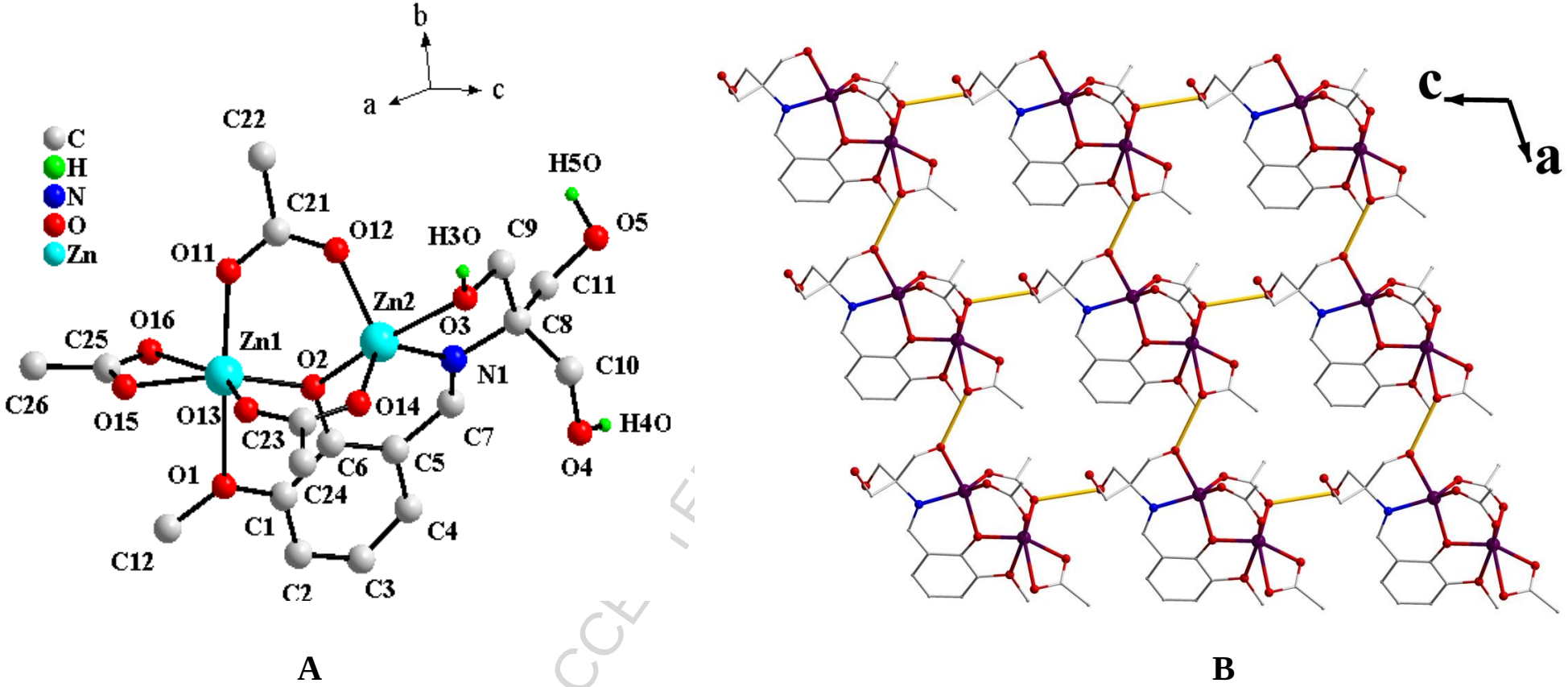

Figure 1

ACCEPTED MANUSCRIPT

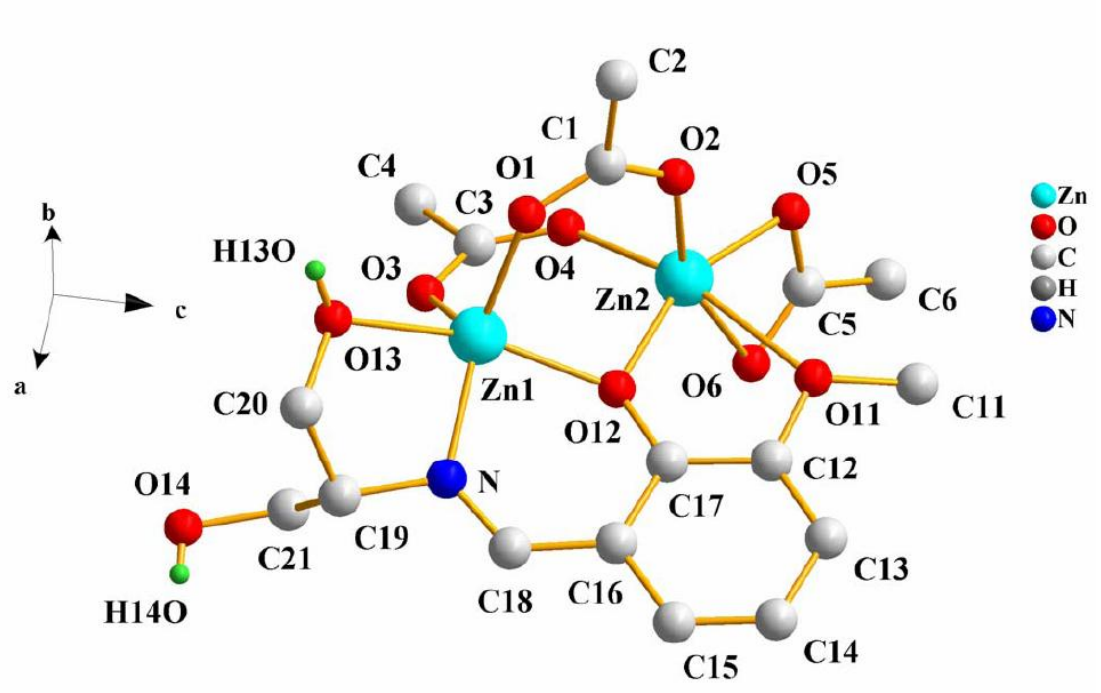

A

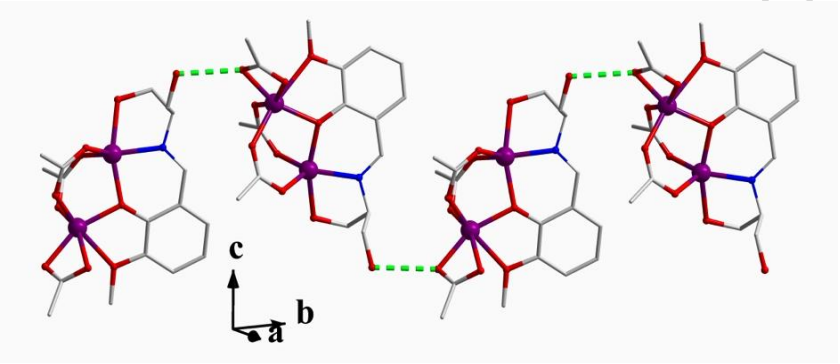

B

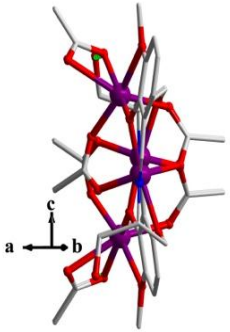

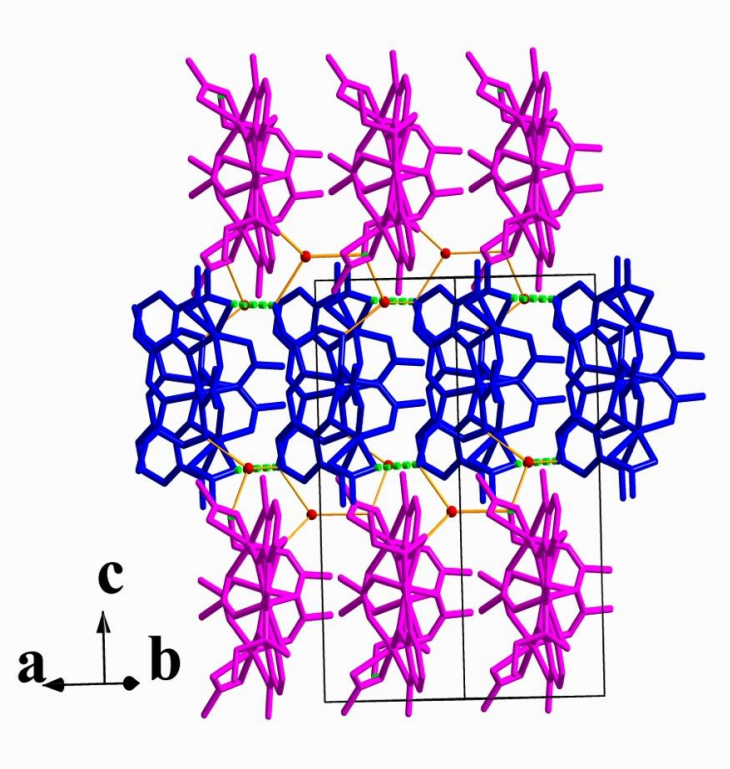

C

Figure 2

ACCEPTED MANUSCRIPT

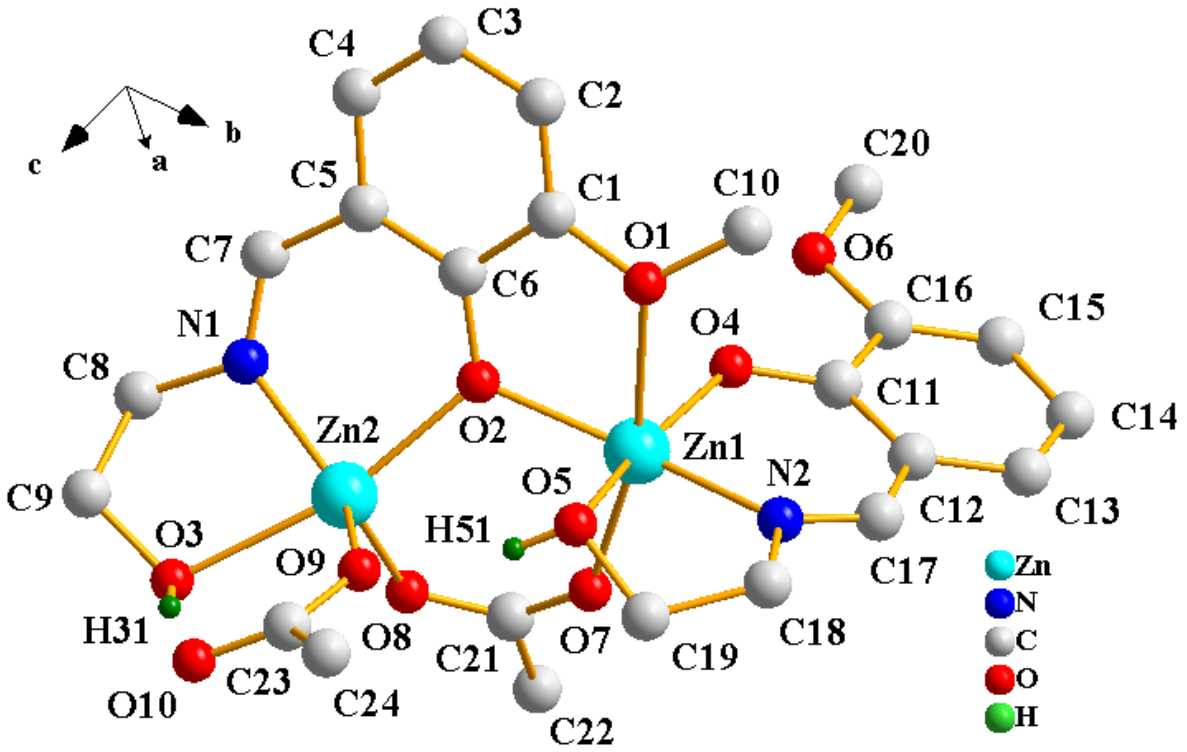

Figure 3

ACCEPTED MANUSCRIPT

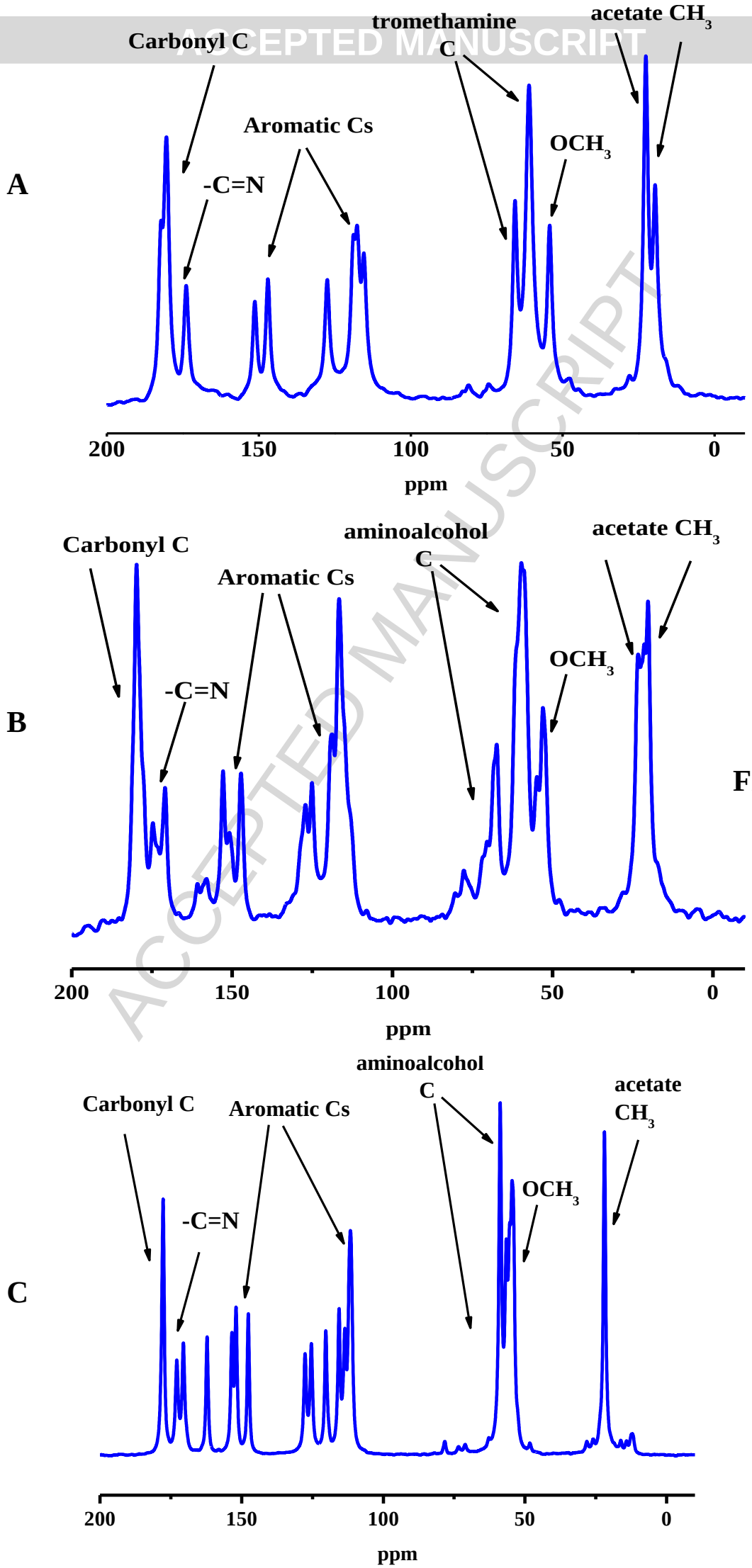

Figure 4

ACCEPTED MANUSCRIPT

ACCEPTED MANUSCRIPT

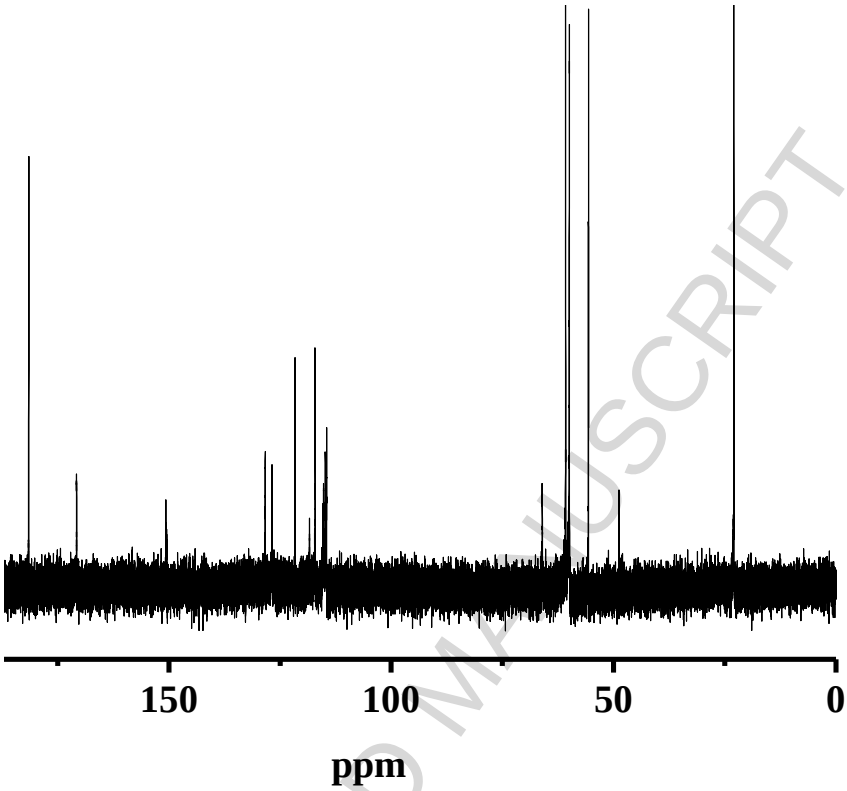

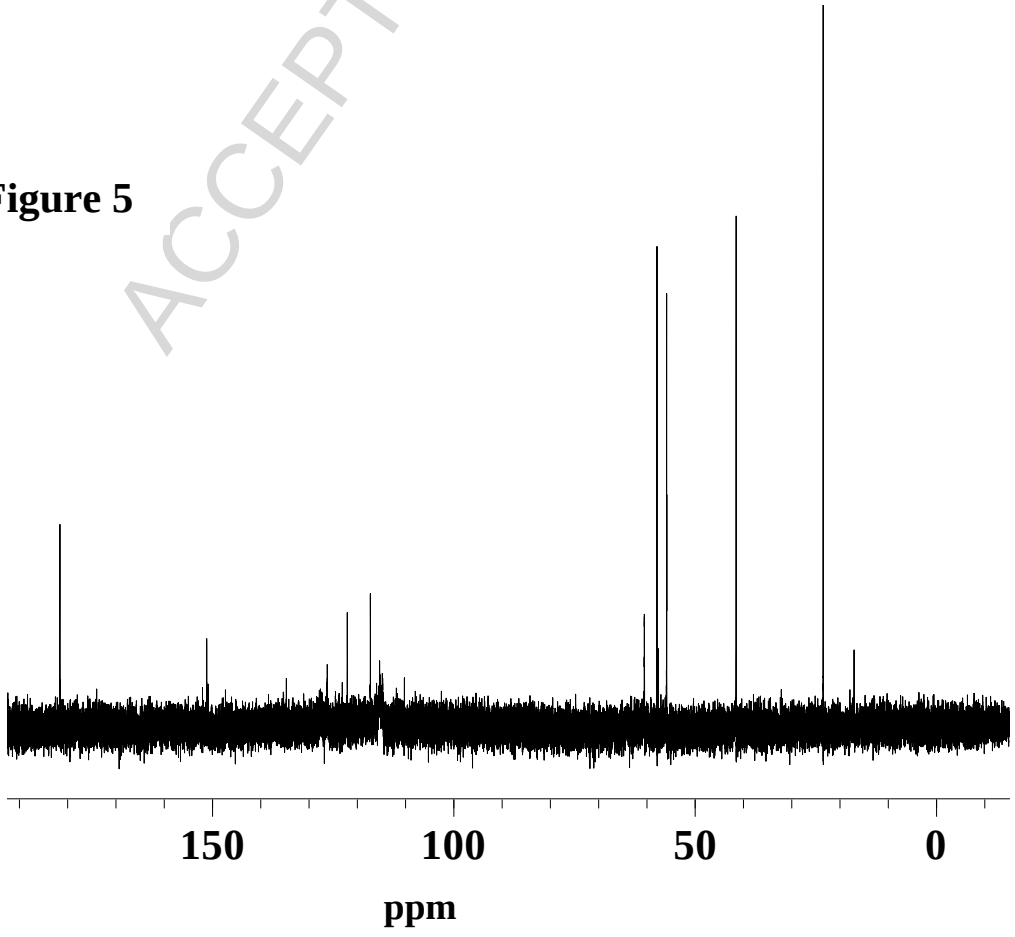

Figure 5

ACCEPTED MANUSCRIPT

A

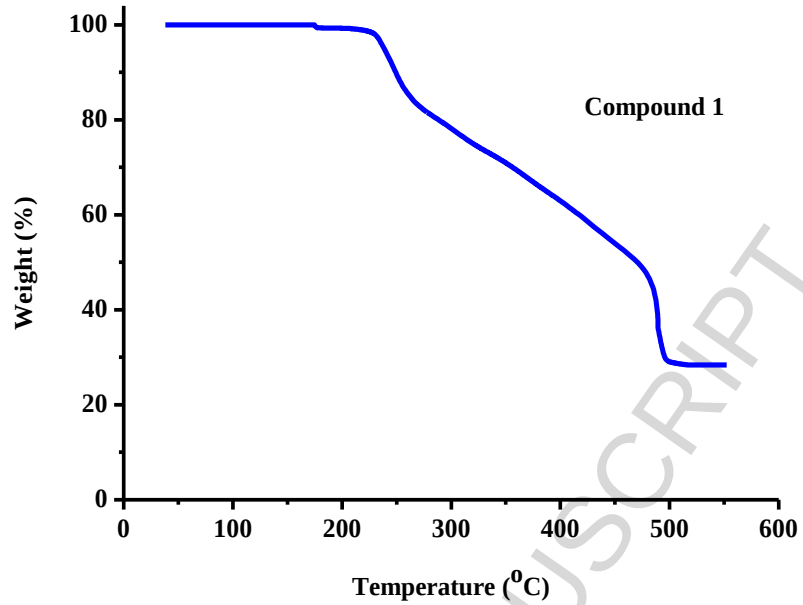

B

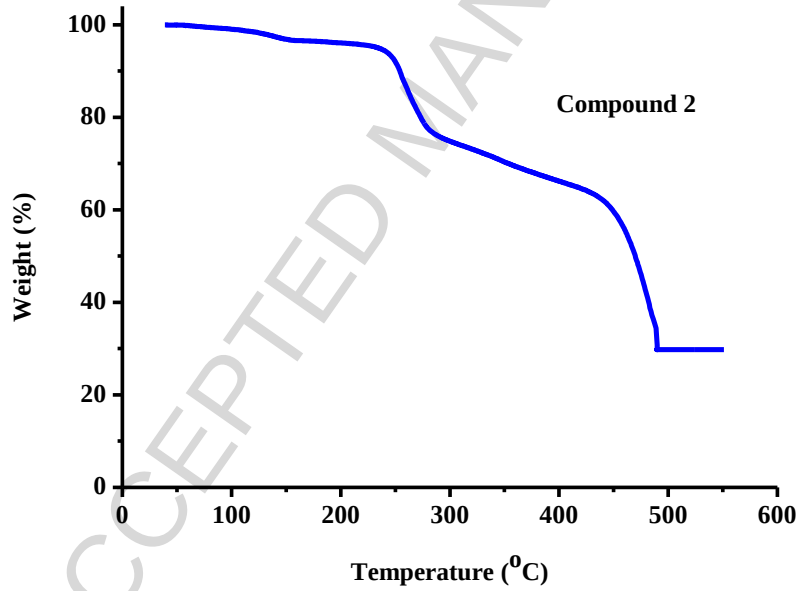

Figure 6

C

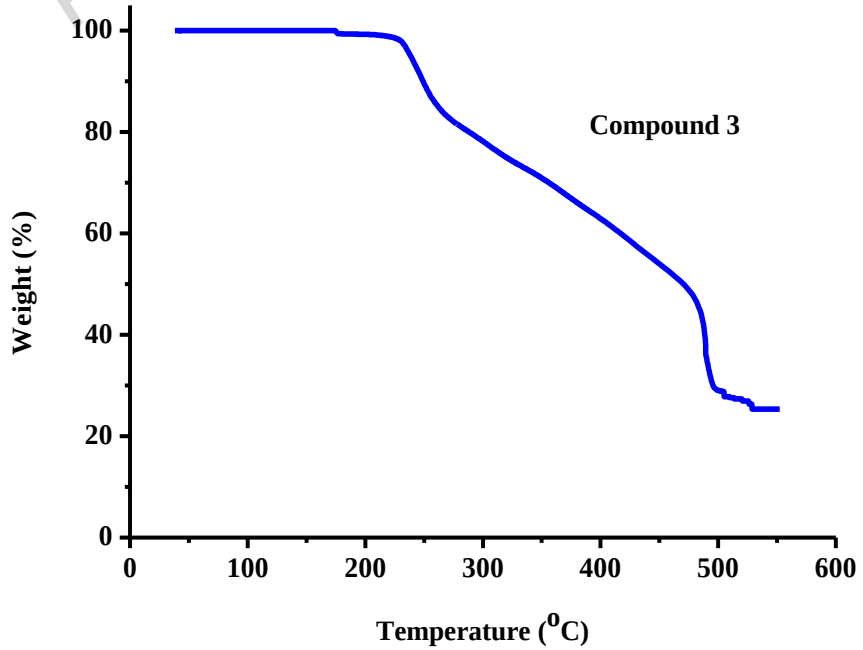

ACCEPTED MANUSCRIPT

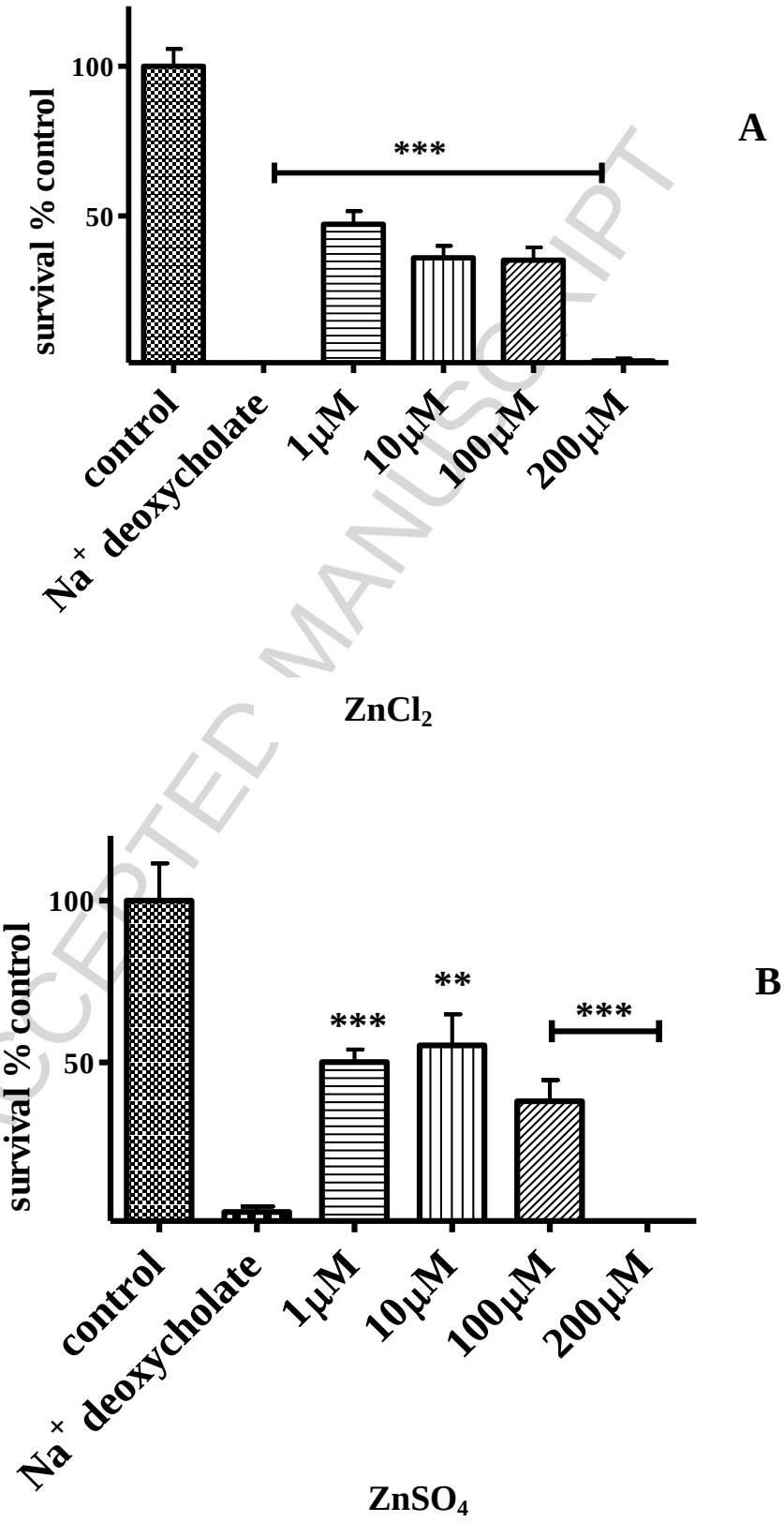

Figure 7

ACCEPTED MANUSCRIPT

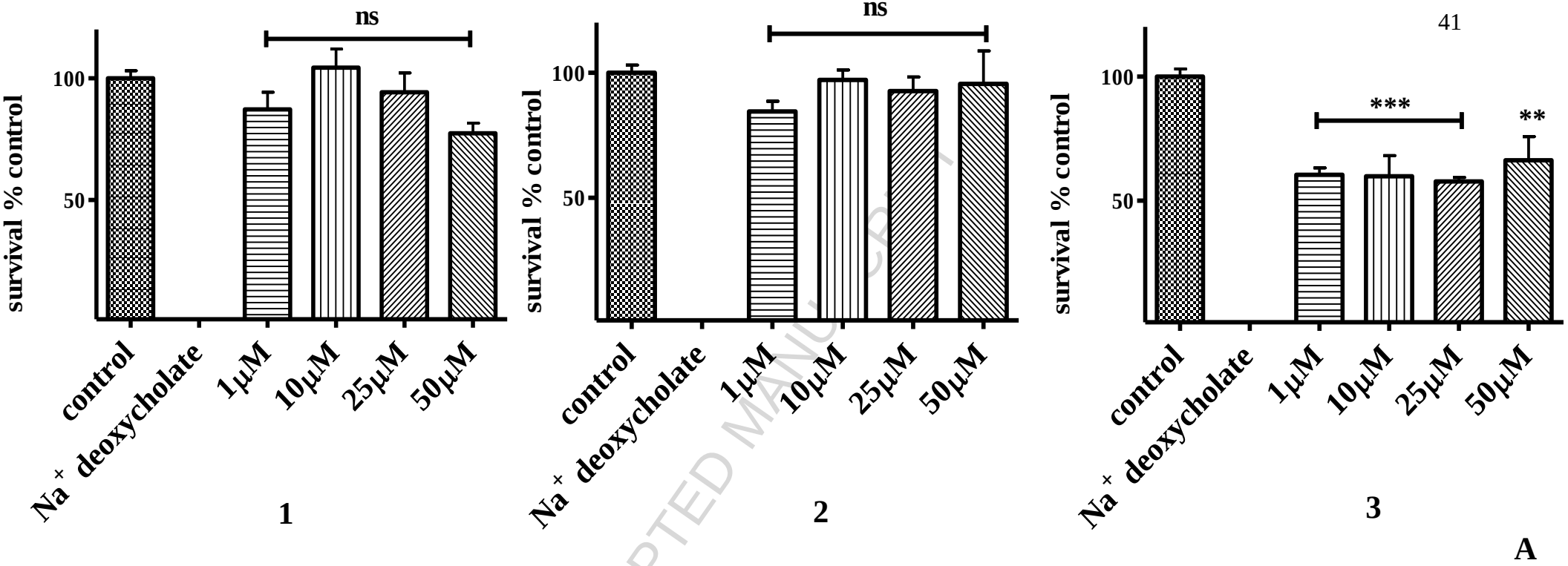

A

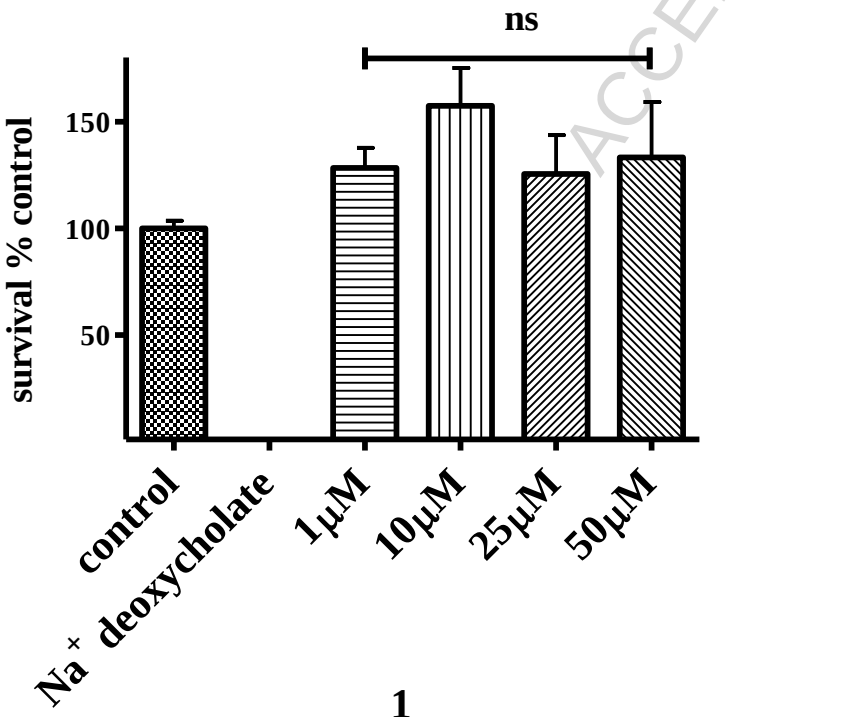

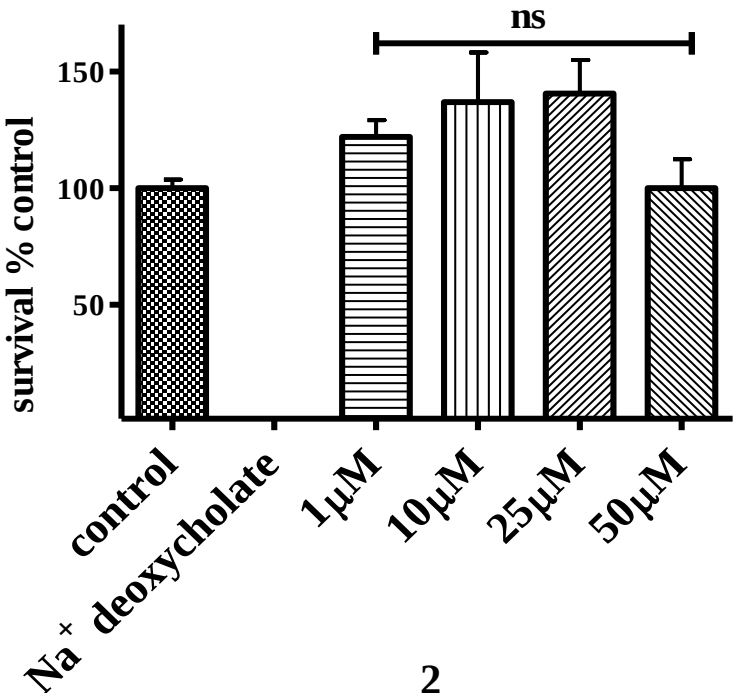

B

Figure 8

ACCEPTED MANUSCRIPT

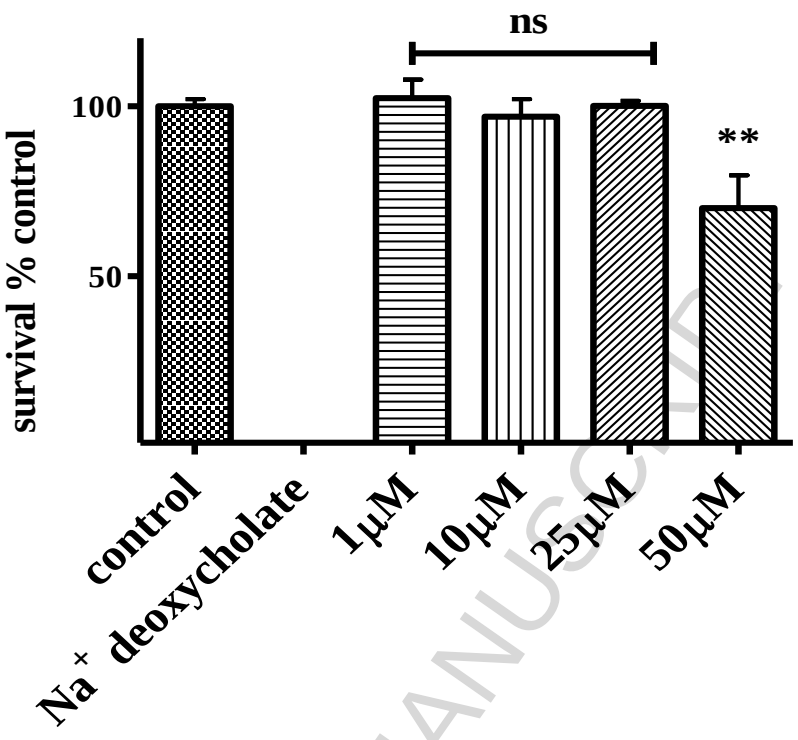

1

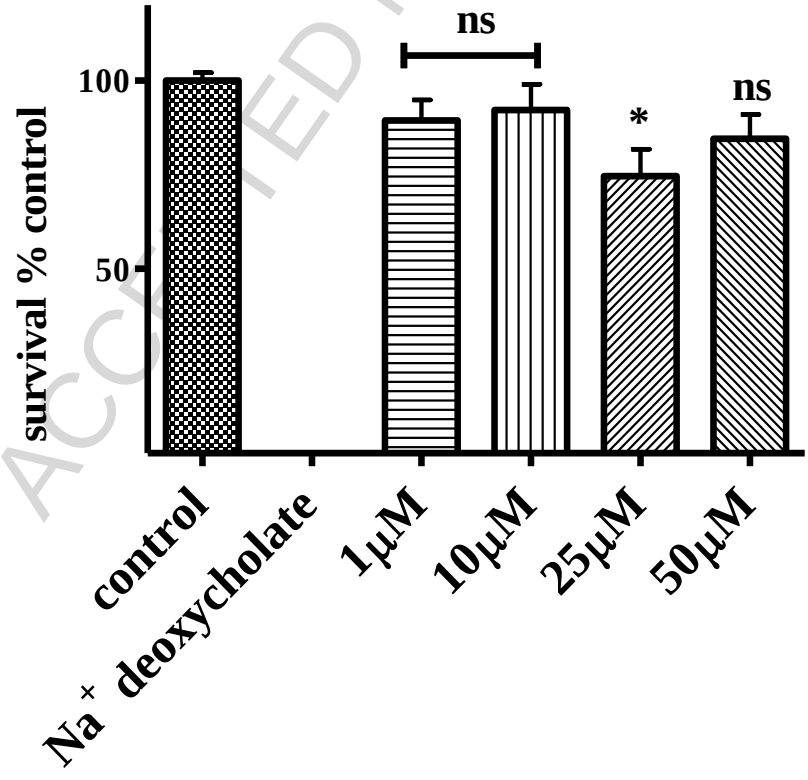

2

Figure 9

ACCEPTED MANUSCRIPT

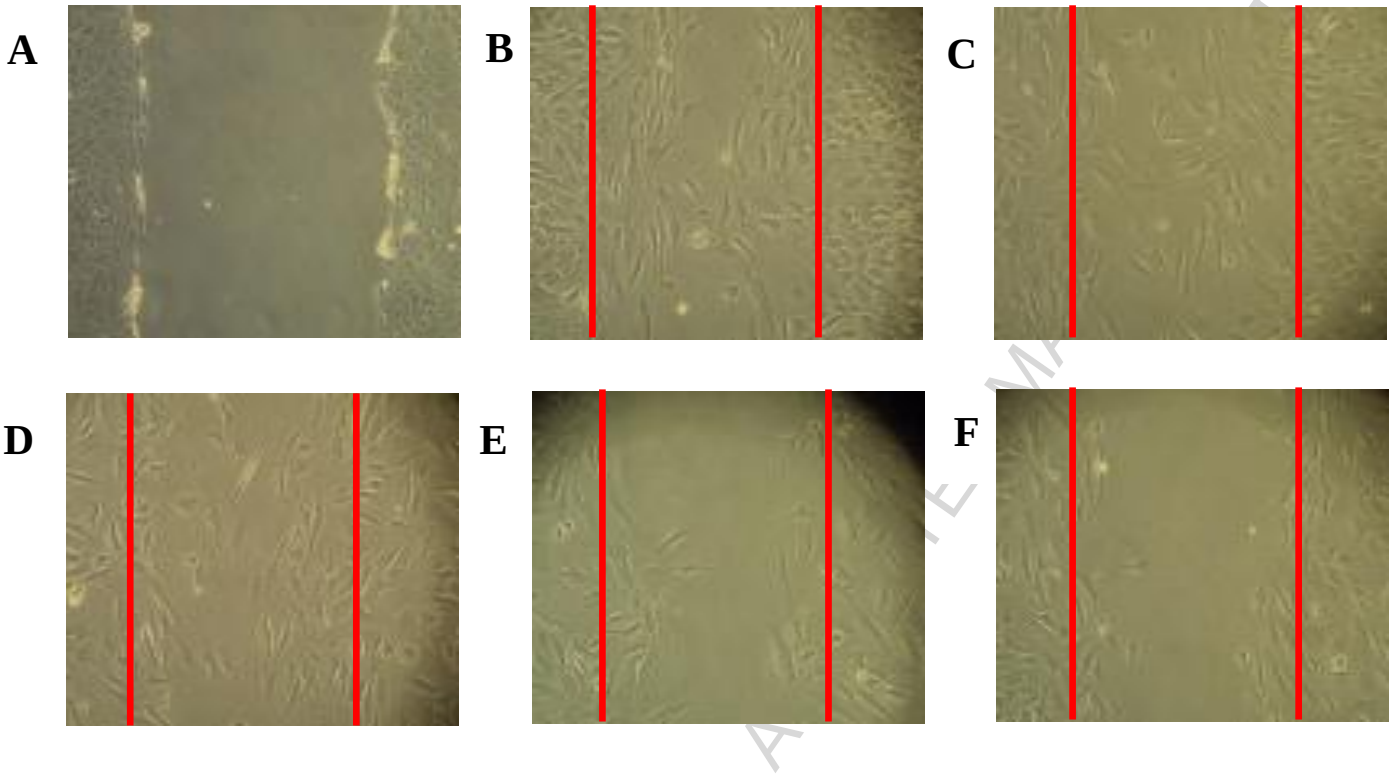

Figure 10

ACCEPTED MANUSCRIPT

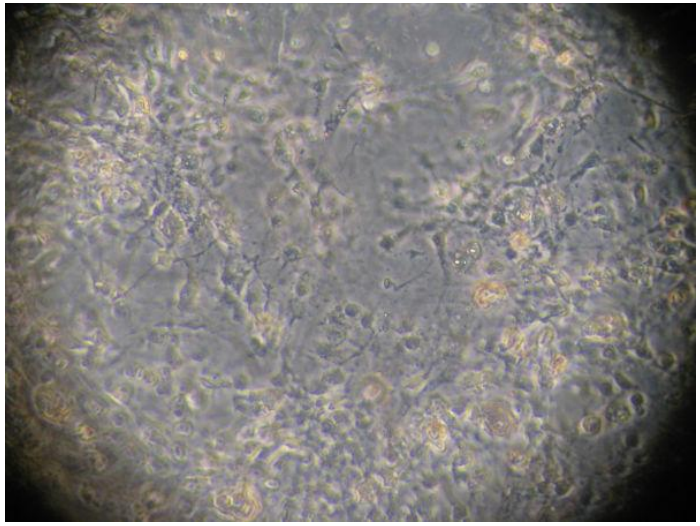

A

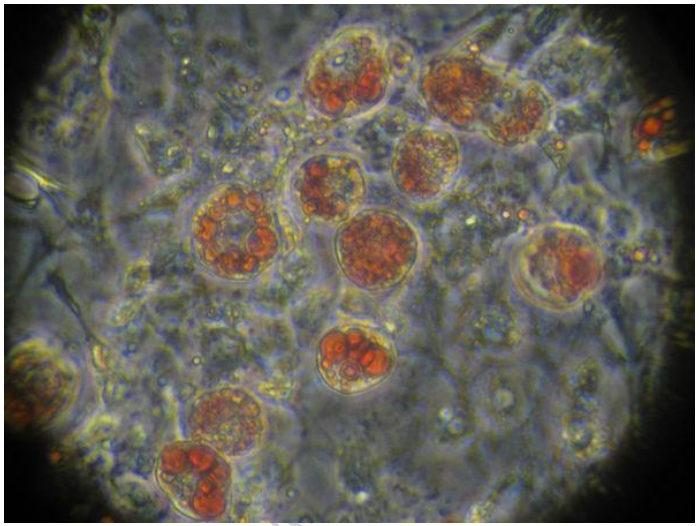

B

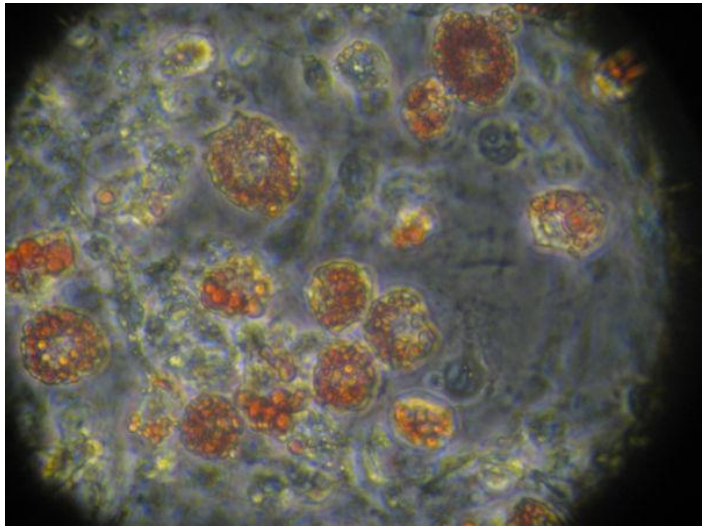

C

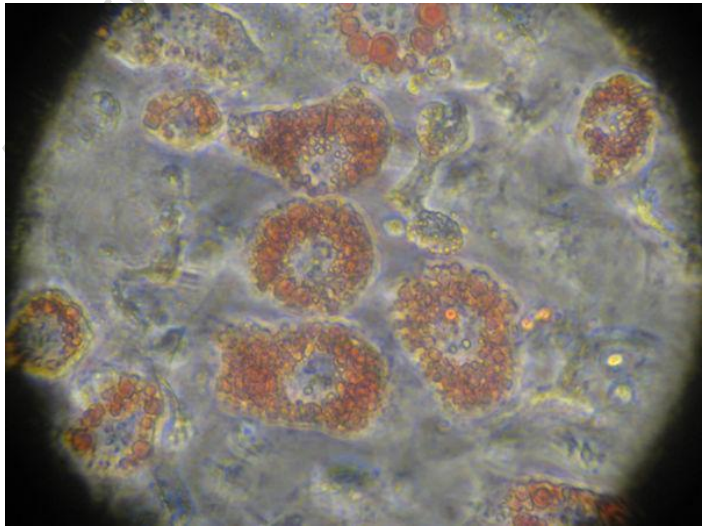

D

Figure 11

ACCEPTED MANUSCRIPT

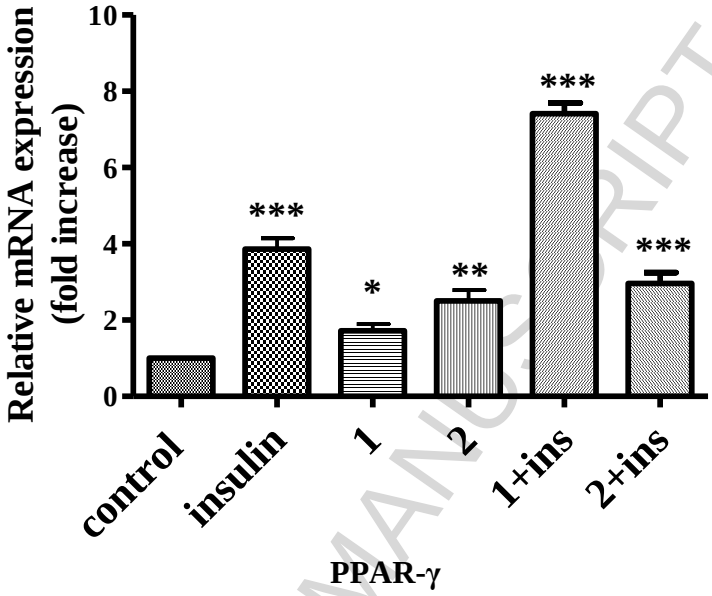

Figure 12

ACCEPTED MANUSCRIPT

ACCEPTED MANUSCRIPT

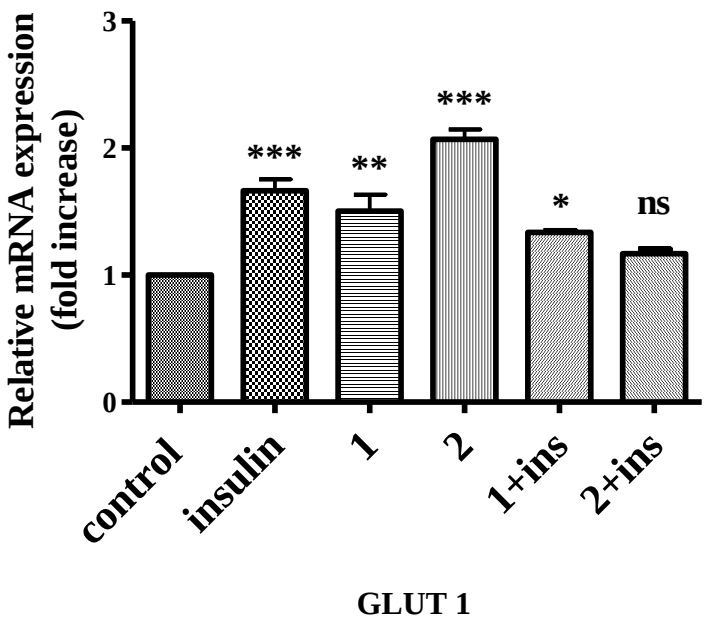

GLUT 1

A

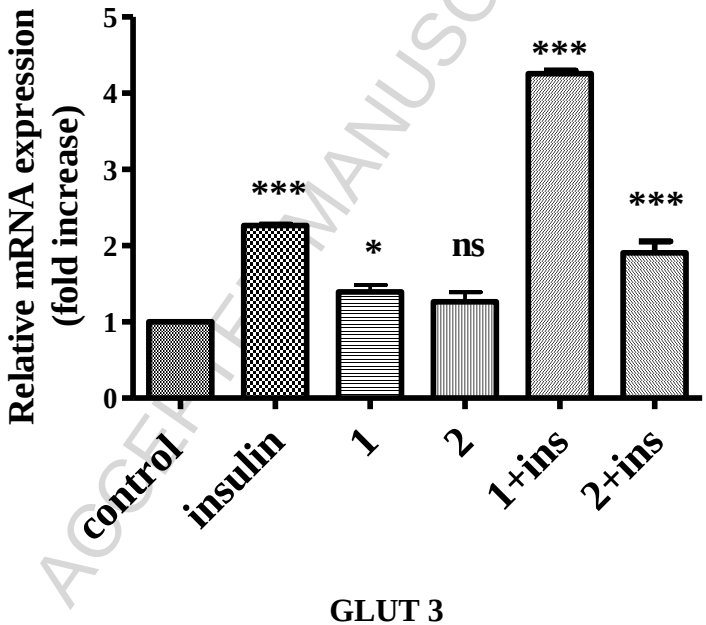

GLUT 3

B

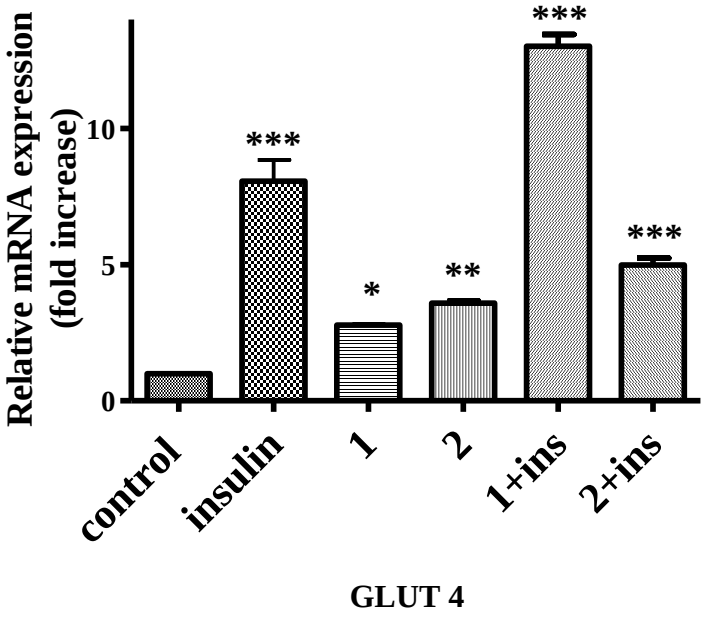

GLUT 4

C

Figure 13

ACCEPTED MANUSCRIPT

Graphical Abstract (Pictogram)

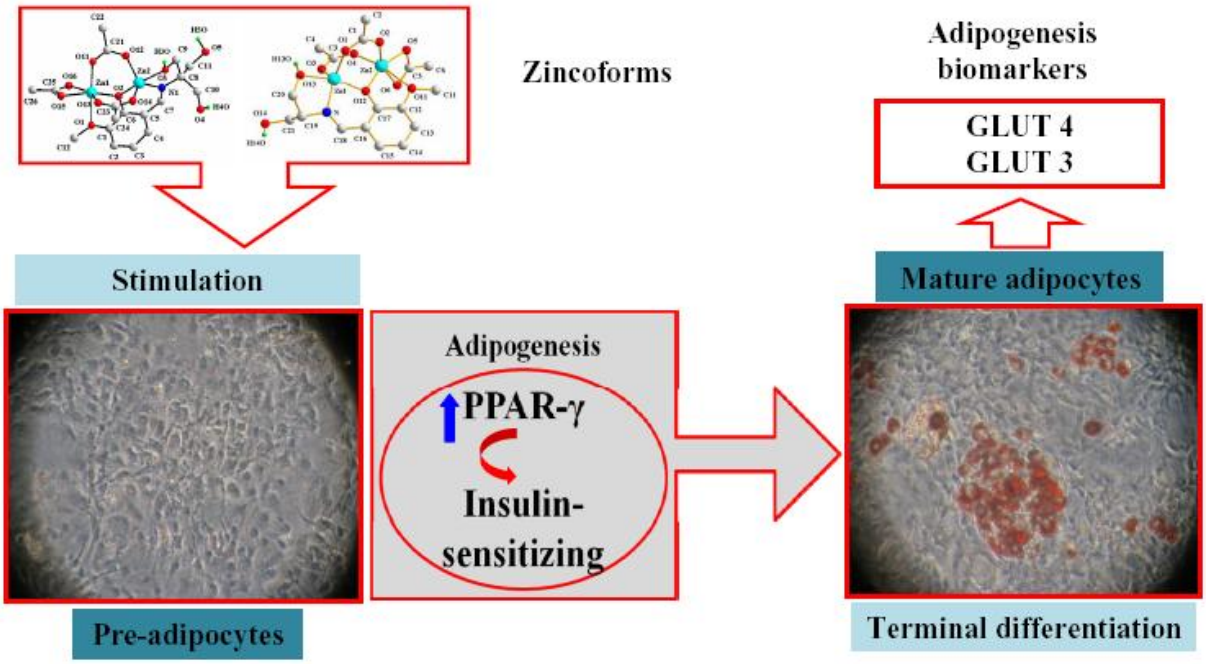

ACCEPTED

ACCEPTED MANUSCRIPT

Graphical Abstract (Synopsis)

Appropriately configured and well-defined ternary zinc-organic (Schiff-base) ligand materials induce 3T3-L1 pre-adipocyte differentiation to mature adipocytes. Structure specificity of the newly synthesized "zincoforms" a) correlates with specific insulin-like bioactivity validated by targeted adipogenic biomarkers, and b) sets the stage for the development of effective "zincodrugs" in Diabetes mellitus II.

ACCEPTED MANUSCRIPT

ACCEPTED MANUSCRIPT

Highlights

- Schiff-base zinc binders bearing vanillin core and terminal alcoholic anchors
- Design, synthesis of well-defined and characterized ternary Zn(II)-Schiff compounds
- Insulin-like Zn(II)-induced 3T3-L1 pre-adipocyte differentiation to a mature state
- Targeted adipogenic biomarkers validate well-defined zincoform lipogenic potential
- Zn-specific adipogenicity reflects insulin-like activity in antidiabetic medication

ACCEPTED MANUSCRIPT